Title: Transcriptomic, clonal, and functional analyses reveal Liver tissue-imprinted immuno-profile of circulating autoreactive CD4 T cells in autoimmune liver diseases.

Authors: Anaïs Cardon[1†], Thomas Guinebretière[1†], Chuang Dong[2], Laurine Gil[2], Sakina Ado[2], Pierre-jean Gavlovsky[1], Martin Braud[1], Richard Danger[1], Christoph Schultheiß[3], Aurelie Domene[4], Perrine Paul-Guilloteaux[4], Caroline Chevalier[5], Laura Bernier[1], Jean-Paul Judor[1], Cynthia Fourgeux[1], Astrid Imbert[6], Marion Khaldi[6, 7], Edouard Bardou-Jacquet[8], Laure Elkrief[9], Adrien Lannes[10], Christine Silvain[11], Mathieu Schnee[12], Florence Tanne[13], Fabienne Vavasseur[5], Lucas Brusselle[1], Sophie Brouard[1], William Kwok[14], Jean-François Mosnier[1, 15], Ansgar Lohse[16], Jeremie Poschmann[1], Masha Binder[3], Jérôme Gournay[1, 6, 7], Sophie Conchon[1§], Pierre Milpied[2§*], Amédée Renand[1§*].

[1] Nantes Université, CHU Nantes, INSERM, Center for Research in Transplantation and Translational Immunology, UMR 1064, F-44000 Nantes, France.

[2] Aix Marseille Université, CNRS, INSERM, Centre d'Immunologie de Marseille-Luminy, CIML, Marseille, France.

[3] Laboratory of Translational Immuno-Oncology, Department of Biomedicine, University and University Hospital Basel, Basel, Switzerland.

[4] MicroPICell facility, SFR-Santé, INSERM, CNRS, Université de Nantes, CHU Nantes, Nantes, France.

[5] Centre d'Investigation Clinique gastro-nutrition, CHU Nantes, Nantes, France.

[6] Service Hepato-gastro-entérologie et Assistance Nutritionnelle, CHU Nantes, Nantes, France.

[7] Institut des Maladies de l'Appareil Digestif, IMAD, CHU Nantes, Nantes, France.

[8] CHU Rennes, Service des maladies du foie, Université Rennes, INSERM, INRAE, Institut NUMECAN, Rennes, France.

[9] CHRU Tours, Service Hépato-Gastroentérologie, Tours, France.

[10] CHU Angers, Service Hépato-Gastroentérologie et Oncologie Digestive, Université d'Angers, Laboratoire HIFIH, UPRES EA3859, SFR 4208, Angers, France.

[11] CHU Poitiers, Service Hépato-Gastroentérologie, Poitiers, France.

[12] CHD Vendée-La Roche sur Yon, Service Hépato-Gastroentérologie, F- 85000, la Roche sur Yon, France.

[13] CHU Brest, Service Hépato-Gastroentérologie, Brest, France.

[14] Center for Translational Immunology, Benaroya Research Institute, Seattle, WA 98101, USA.

[15] Service Anatomie et Cytologie Pathologiques, CHU Nantes, Nantes, France.

[16] First Department of Medicine, University Medical Center Hamburg-Eppendorf, Hamburg, Germany.

[†] Equal contribution

[§] Equal contribution, co-last

* Corresponding authors : Dr Amédée Renand, INSERM UMR1064 – Center for Research in Transplantation and Translational Immunology, CHU Nantes – Hôtel Dieu, 30 boulevard Jean Monnet, 44093, Nantes Cedex 01, France. Phone: (+33)240087410. E-mail address: amedee.renand@univ-

nantes.fr ; Dr Pierre Milpied, INSERM, Centre d'Immunologie de Marseille- Parc scientifique et technologique de Luminy, 13288, Marseille, France. Phone : (+33)491269406. E-mail address: milpied@ciml.univ-mrs.fr

Abstract.

Autoimmune liver diseases (AILD) are immune-mediated disorders in which CD4 T cells may play a central role. However, self-antigen-specific CD4 T cells are mainly characterized in the bloodstream, and the link with the immune response in the targeted tissue is a difficult and under-studied task in AILD. We hypothesize that circulating self-antigen-specific CD4 T cells contain dominant hepatic CD4 T cell clonotypes and represent liver-derived autoreactive CD4 T cells. Single cell transcriptomic analysis of circulating self-antigen-specific CD4 T cells reveal a specific B-helper and immuno-exhausted transcriptional profile, which is conserved for different autoantigens, but distinct from several other types of foreign antigen specificities. The dominant hepatic CD4 T cell clones shared a similar transcriptomic signature and were enriched in the circulating PD1+ TIGIT+ HLA-DR+ CD4 T cell subset. In liver biopsy, PD1+ CD4 T cells were present in tertiary lymphoid structure, reinforcing the hypothesis of a pathogenic role of these cells. Using a mouse model, we demonstrated antigen-specific CD4 T cells acquired the immuno-exhausted transcriptional profile when they accumulated in the liver after local antigen reactivity. Inhibition of immune checkpoint molecules contributed to increased hepatic damages in a CD4 T cell dependent manner. This study reveals the origin of liver-autoreactive CD4 T cells in the blood of AILD patients that are imprinted by the liver environment and recirculate from the damaged tissue during the active phase of the disease. In addition, this study also shows how immune checkpoint molecules contribute to local antigen-specific tolerance in the liver, which may be dysregulated in AILD and immunotherapy-induced acute hepatitis. Finally, our study enables tracking and isolating liver autoreactive CD4 T cells in future diagnostic and therapeutic purposes.

Introduction.

Autoimmune liver diseases (AILD) are rare immune-mediated chronic inflammatory diseases. The three main AILD are autoimmune hepatitis (AIH), primary biliary cholangitis (PBC) and primary sclerosing cholangitis (PSC), which are characterized by the destruction of the liver parenchyma (hepatocyte destruction), the intrahepatic biliary epithelial cells (cholangiocytes) of small bile ducts or the intra- or extra-hepatic biliary epithelial cells of the large bile ducts, respectively. AIH, PBC and PSC are characterized by immune infiltrate in the liver. In AIH, the parenchyma and portal-tract are affected, and interface hepatitis is a characteristic of this disease[1,2]. In PBC, portal-tract inflammation with lymphocytes and plasma cells with loss of bile ducts has been described[3,4]. During PSC, immune infiltrate is detectable in the liver and the biliary tree[5–7]. Autoantibodies are detectable in the serum of the patients, especially for AIH and PBC. PSC is a more complex disease often associated with ulcerative colitis[8]. Elevated immunoglobulin (IgG) levels are a hallmark of AIH, and this disease is controlled by immunosuppressive (IS) therapies, which are not used or effective in PBC and PSC. Only in case of overlap syndrome with AIH, PBC and PSC patients received IS treatments. In AIH and overlap syndrome, the relapse rate is high after treatment withdrawal, suggesting the persistence of therapy resistant autoimmune factors. Although all three AILD are classified as autoimmune diseases, the degree of intensity of the autoreactive response appears to be variable, and the link with the autoimmune T-cell signature is unknown. In our study, we focused primarily on AIH and PBC diseases.

In AILD, the strong association with the HLA locus, the presence of autoantibodies in serum and T cells in damaged tissue reflects the complete adaptive immune response against self-antigens, with a possible central role for CD4 T cells with their helper function[9–12]. The recent demonstration of the efficacy of rituximab (anti-CD20) treatment in AIH confirms that B cells contribute to the pathogenesis

of AILD[13]. However, it is difficult to establish the in-depth immune profile of autoreactive CD4 T cells, as they are rare in the blood and not all self-antigens are known. During AILD, some target self-antigens are described. Anti-SLA antibodies target the Sepsecs self-antigen, anti-LKM1 target the CYP2D6 self-antigen, anti-LC1 target the FTCD self-antigen and the anti-mitochondrial M2 (anti-M2) antibody target the PDCE2 self-antigen. T cell reactivity against Sepsecs, CYP2D6, FTCD and PDCE2 is detectable in the blood of AILD patients with a preferential Th1 cytokine profile (IFNG)[14–17]. In a mouse model, immunization against CYP2D6 or FTCD induces liver autoimmunity[18–21]. Those studies reinforce the idea of a complete adaptive immune response against self-antigens in AILD with a central role of CD4 T cells. Recently, we were able to characterize the single cell transcriptomic profile of Sepsecs-specific CD4 T cells in the blood of AIH patients with anti-SLA antibodies[22]. Compared to Candida Albicans-specific CD4 T cells, Sepsecs-specific CD4 T cells were PD1+ CXCR5- cells and expressed high level of the B-helper gene, *IL21*, as well as the *IFNG* gene and the immunoregulatory genes *TIGIT* and *CTLA4,* among others. In the blood of AIH patients, we found an increase in IL21- and IFNG-producing PD1+ CXCR5- CD4 T cells, independent of the presence of specific autoantibodies (e.g anti-SLA)[22]. The signature of these autoreactive CD4 T cells in the blood presented high similarity with the peripheral T helper cells (TPH) identified in the synovium of patients with rheumatoid arthritis and in other tissues during autoimmunity[23–29]. However, it was still unknown whether the TPH immune signature was a common feature of other liver-self-antigen-specific CD4 T cells.

The similarity between circulating Sepsecs-specific CD4 T cells and TPH in the tissue raised the question whether circulating autoreactive CD4 T cells are directly linked to the reactivity in the tissue. Although TPH cells can also be found in smaller numbers in the blood, the site of their differentiation is unknown[22,23,30]. In liver biopsies from AIH and PBC patients, Sepsecs- and PDCE2-reactive T cells are detectable but poorly characterized; they produce TNF and/or INFG[31–34]. Characterizing the immune signature of T cells in tissues is a hot topic, but the dynamic link between tissues and circulation is less well understood, particularly for CD4 T cells. Liver biopsies are small and rare biological material making difficult the characterization of liver-autoreactive CD4 T cells during AILD in the tissue. Thus, the capacity to detect in the blood autoreactive cells directly linked to tissue pathogenesis is an interesting perspective. Following an immune response or infection, peripheral CD4 and CD8 T cells can migrate into tissues to differentiate into tissue-resident memory (TRM) cells that is associated with clonal retention and segregation in the tissue[35,36]. Interestingly, TRM CD4 T cells, TPH cells and circulating Sepsecs-specific CD4 T cells express high levels of immune checkpoint molecules (PD1, TIGIT and CTLA4) but also *PRDM1, TOX* and other genes. This may suggest a tissue imprint of TPH and Sepsecs-specific CD4 T cells found in the peripheral circulation due to chronic antigen stimulation in the tissue. We thus hypothesized that some circulating autoreactive CD4 T cell derive from an aberrant clonal expansion in the tissue during active autoimmunity.

Here we used integrative single-cell immuno-transcriptomics to characterize three distinct liver-self-antigen-specific CD4 T cell reactivities and expanded intrahepatic CD4 T cell clonotypes in the blood of AILD patients. We revealed a shared signature and demonstrated that liver-autoreactive CD4 T cells can be detected in the peripheral bloodstream. In a mouse model designed to study the initiation of an immune response against an antigen expressed in the liver, we observed alterations of the transcriptomic profile of intrahepatic antigen-specific CD4 T cells after local antigen reactivity. The most relevant markers characterizing both intrahepatic and circulating liver-autoreactive CD4 T cells were the immune checkpoint molecules TIGIT, PD1 and CTLA-4, which were involved in the control of local antigen-specific T cell reactivity. These results demonstrate how circulating liver-self-antigen-specific CD4 T cells are linked to tissue auto-reactivity and how the hepatic environment imprints their immune signature, with an important clinical perspective for monitoring and targeting liver auto-reactivity.

129 **Methods:**

130 **Patients**

131 All the patients eligible signed a written informed consent prior to inclusion into a bio-bank of samples
132 from AILD patients (BIO-MAI-FOIE) maintained in Nantes University Hospital which obtained regulatory
133 clearance from the biomedical research Ethics Committee (CPP) and all required French Research
134 Ministries authorizations to collect biological samples (ref MESR DC-2017-2987). The biobank is
135 supported by The HEPATIMGO network promoted since 2017 (RC17_0228) by Nantes University
136 Hospital and is a prospective Multi-centric collection managed by the Biological Resource center of the
137 CHU of Nantes. All data collected were treated confidentially and participants are free to withdraw
138 from the study at any time, without explanation and without prejudice to their future care. It was
139 granted authorization from the CNIL: 2001209v0). All AIH patients included in this study had a
140 simplified diagnostic score superior or equal to 6 according to the simplified scoring system for AIH of
141 the international autoimmune hepatitis group (IAHG)[2,37]. PBC patients included in this study were
142 diagnose based on cholestasis, increase serum IgM and presence of anti-mitochondria M2 (anti-M2)
143 antibody[4]. Active AIH (AIHa) patients are untreated patients with new onset AIH patients enrolled at
144 diagnosis prior any treatment initiation as previously described[38], and AIH patients under standard
145 treatment but do not normalize the transaminases (AST and ALT) and/or the serum IgG levels or are
146 under relapsing event. Remission AIH (AIHr) patients are defined biochemically by a normalization of
147 the transaminases and the IgG levels, according to the most recent European clinical practice
148 guidelines on AIH [2]. All NASH (non-Alcoholic SteatoHepatitis) patients had histological evidence of
149 NASH and had dysmetabolic syndromes. This study was carried out in accordance with the Principles
150 of International Conference on Harmonisation (ICH) Good Clinical Practice (GCP) (as adopted in France)
151 which builds upon the ethical codes contained in the current version of the Declaration of Helsinki, the
152 rules and recommendations of good international (ICH) and French clinical practice (good clinical
153 practice guidelines for biomedical research on medicinal products for human use) and the European
154 regulations and/or national legislation and regulations on clinical trials.

155 **Peptide re-stimulation assay**

156 10 to 20x10^6 PBMCs (at a final concentration of 10x10^6/mL) were stimulated for 3 to 4h at 37°C with
157 1µg/mL of synthesized peptides spanning all of the Sepsecs, CYP2D6 or PDCE2 sequences (20 amino
158 acids in length with a 12 amino acid overlap; Synpeptide, China) or with 1µg/mL of PepTivator^R C.
159 albicans MP65, Influenza A (H1N1) MP1 and SARS-CoV-2 Prot_S (SPIKE) (peptides pools of 15 amino
160 acids length with 11 amino acid overlap, Miltenyi Biotec) in 5% human serum RPMI medium in the
161 presence of 1µg/ml anti-CD40 (HB14, Miltenyi Biotec). After 3 to 4 hrs of specific peptide stimulation,
162 PBMCs were first labeled with PE-conjugated anti-CD154 (5C8, Miltenyi Biotec) and CD154$^+$ cells were
163 then enriched using anti-PE magnetic beads (Miltenyi Biotec). A 1/10th fraction of non-enriched cells
164 was saved for frequency determination. Frequency was calculated with the formula F = n/N, where n
165 is the number of CD154 positive cells in the bound fraction after enrichment and N is the total number
166 of CD4+ T cells (calculated as 10 × the number of CD4+ T cells in 1/10th non-enriched fraction that was
167 saved for analysis). After enrichment, cells were stained with appropriate antibodies (Supplementary
168 table 1).

169 **Tetramer staining**

170 For tetramer staining, 30 million PBMCs in 200 µL of 5% human serum RPMI medium were stained
171 with 20 µg/mL PE-labeled tetramers at room temperature for 100 minutes. Cells were washed and
172 incubated with anti- PE magnetic beads (Miltenyi Biotec, Germany) at 48C for 20 minutes, and a one-
173 tenth fraction was saved for analysis. The other fraction was passed through a magnetic column
174 (Miltenyi Biotec). After enrichment, cells were stained with appropriate antibodies (Supplementary
175 table 1). $Sepsecs_{187-197}$ HLA-DRB1 03:01 tetramer was generated by the tetramer core at the Benaroya
176 research institute (Seattle, USA).

177 **Flow cytometry and cell sorting**

178 All antibodies used are described in the supplementary table 1. Briefly, for surface staining, PBMCs
179 were incubated 20 minutes with a mix of antibodies and then washed prior analysis or cell sorting on
180 BD FACSCantoII, Cytek Aurora or BD FACSAriaII. For intra-cellular staining we used the
181 Fixation/Permeabilization Solution Kit (BD Cytofix/Cytoperm™, BD Biosciences).

182 **Single cell RNA sequencing and analysis (plate-based assays)**

183 For scRNA-seq analysis of peptide-restimulated CD4 T cells, $CD154^+$ memory CD4 T cells were first
184 sorted on BD FACSAriaII, one cell per well, in 96-well plates containing specific lysis buffer at the CRTI,
185 Nantes. Plates were immediately frozen for storage at -80°C, and sent on dry ice to the Genomics core
186 facility of CIML, Marseille, for further generating scRNAseq libraries with the FB5P-seq protocol as
187 described[22,39]. Briefly, mRNA reverse transcription (RT), cDNA 5'-end barcoding and PCR amplification
188 were performed with a template switching (TS) approach. After amplification, barcoded full-length
189 cDNA from each well were pooled for purification and library preparation. For each plate, an Illumina
190 sequencing library targeting the 5'-end of barcoded cDNA was prepared by a modified transposase-
191 based method incorporating a plate-associated i7 barcode. Resulting libraries had a broad size
192 distribution, resulting in gene template reads covering the 5'-end of transcripts from the 3rd to the 60th
193 percentile of gene body length on average. As a consequence, sequencing reads covered the whole
194 variable and a significant portion of the constant region of the TCRα and TCRβ expressed mRNAs,
195 enabling assembly and reconstitution of TCR repertoire from scRNAseq data. Libraries prepared with
196 the FB5P-seq protocol were sequenced on Illumina NextSeq2000 platform with P2 100-cycle kits,
197 targeting $5x10^5$-$1x10^6$ reads per cell in paired-end single-index mode with the following configuration:
198 Read1 (gene template) 103 cycles, Read i7 (plate barcode) 8 cycles, Read2 (cell barcode and Unique
199 Molecular Identifier) 16 cycles. We then used a custom bioinformatics pipeline to process fastq files
200 and generate single-cell gene expression matrices and TCR sequence files, as described[22,39].

201 For scRNA-seq of tetramer-stained CD4 T cells, we used an updated version of FB5P-seq (Flash-FB5P-
202 seq) modified to implement advances developed by Hahaut et al. in the Flash-seq protocol[40]. Cells were
203 sorted in 2 µl lysis mix composed of 0.1% Triton X-100 (0.02 µl), 1.2 U/µl recombinant RNAse inhibitor
204 (0.06 µl), 6 mM dNTP mix (0.48 µl), 1.6 mM RT primer (5'-
205 TGCGGTATCTAAAGCGGTGAGTTTTTTTTTTTTTTTTTTTTTTTTTTTTTT*V*N-3') (0.36 µl), 0.0125 pg/µl
206 ERCC spike-in mix (0.05 µl), 9 mM dCTP (0.18 µl), 1 M betaine (0.4 µl), 1.2 mM DTT (0.024 µl) and PCR-
207 grade H_2O (0.426 µl). Plates were conserved at -80°C until sorting, thawed at RT for cell sorting, and
208 immediately refrozen on dry ice then conserved at -80°C until further processing. Reverse transcription
209 with template switching and cDNA amplification were performed in a single step. Each plate containing
210 cells in lysis mix was thawed on ice, heated at 72°C for 3 min then immediately placed on ice. To each
211 well containing 2 µl cell lysate, we added 8 µl of an RT-PCR mix composed of 2 U/µl Superscript IV

212 reverse transcriptase (0.1 µl), 0.8 U/µl recombinant RNAse inhibitor (0.2 µl), 1X KAPA HiFi ReadyMix (5
213 µl), 4.8 mM DTT (0.48 µl), 0.8 M betaine (1.6 µl), 9.2 mM $MgCl_2$ (0.092 µl), 0.1 µM forward PCR primer
214 (5'-AGACGTGTGCTCTTCCGAT*C*T-3') (0.1 µl), 0.1 µM reverse PCR primer (5'-
215 TGCGGTATCTAAAGCGGTG*A*G-3') (0.1 µl), 1.84 µM biotinylated barcoding template switching
216 oligonucleotide (5'-biotin-AGACGTGTGCTCTTCCGATCTXXXXXXXXNNNNNNNNCAGCArGrGrG-3', where
217 XXXXXXXX are well-specific barcodes as published[39], NNNNNNNN are random nucleotides serving as
218 Unique Molecular Identifiers, and rG are riboguanosine RNA bases) (0.184 µl) and PCR-grade H_2O
219 (0.144 µl). Then plates were incubated in a thermal cycler 60 min at 50°C, 3 min at 98°C, and 22 cycles
220 of 20 sec at 98°C, 20 sec at 67°C and 6 min at 72°C. We then pooled 5 µl amplified cDNA from all wells
221 into one tube per plate, and performed 0.6X SPRI bead-based purification. Sequencing libraries were
222 prepared from 800 pg cDNA per plate with the Illumina Nextera XT protocol, modified to target
223 sequencing reads to the 5' end of cDNA, as described [ref]. Before sequencing, pooled indexed libraries
224 were depleted from ribosomal RNA-derived cDNA molecules by using the SEQoia RiboDepletion Kit
225 (Biorad) according to the manufacturer's instructions. Flash-FB5P-seq libraries were sequenced on an
226 Illumina NextSeq2000 using P3 100 cycle kit and targeting $5x10^5$-$1x10^6$ reads per cell in paired-end
227 single-index mode with the following configuration: Read1 (gene template) 114 cycles, Read i7 (plate
228 barcode) 8 cycles, Read2 (cell barcode and Unique Molecular Identifier) 16 cycles. We then used a
229 custom bioinformatics pipeline to process fastq files and generate single-cell gene expression matrices
230 and TCR sequence files. Briefly, reads were processed with the zUMIs pipeline[42] to generate the gene
231 expression UMI count matrix, and with the TRUST4 pipeline[44] to reconstruct TCR sequences.

232 Quality control excluded cells with more than 10% mitochondrial UMIs, less than 400 genes, more than
233 25% ERCC UMIs, less than 0.7 ERCC spike-in quantification accuracy[39], and less than 5% ribosomal
234 protein coding UMIs. Gene expression UMI matrices were analyzed with the *Seurat v4.1.0* package in
235 R v4.1.2 using standard log normalization, 4,000 highly variable genes (computed with the *vst* method)
236 from which we removed all TCR coding genes, 40 principal components for computing UMAP and
237 Louvain clustering at resolution 0.8. Marker genes of unsupervised clusters or metadata-defined
238 clusters were computed with the *FindAllMarkers* function using Wilcoxon test with an adjusted p-value
239 cutoff of 0.01. Gene expression heatmaps were generated with the *pheatmap* function. TCR
240 clonotypes were computed and analyzed as described previously[22].

241 **Single cell RNA sequencing and analysis (10x Genomics protocol)**

242 First, PD-1^+CD45RA^-CXCR5^- and PD-1^-CD45RA^-CXCR5^- CD4 T cells were sorted on BD FACSAriaII. Cells
243 were counted, centrifuged (500g, 5 min, 4°c) then resuspended at the recommended dilution for a
244 20000 cell loading per sample onto a Next GEM Chip K (PN-1000286) and run on a Chromium Single
245 Cell Controller using the Chromium Single Cell 5' V2 Next GEM single cell kit (PN-1000263) according
246 to the manufacturer's instructions (CG000331, 10× Genomics). Gex and VDJ-TCR libraries were then
247 prepared (PN-1000190, PN-1000252, PN-1000215 also from 10X genomics), checked for quality
248 controls and sequenced on a S2 flow cell on a Nova-Seq 6000 (Illumina) at the GenoBird platform (IRS-
249 UN, CHU Nantes). Raw reads were analyzed using FastQC for quality controls and were then processed
250 using CellRanger pipeline (v3.1.0 with default parameters). Generated FASTQ files were aligned to the
251 human reference genome GRCh38.

252 The base calling has been done using Illumina bcl2fastq2 (v2.20). The FASTQs obtained has been
253 analyzed for cell identification and UMIs count using 10x Genomics Cell Ranger 7.0.1 and hg38
254 reference. Four filtered matrices were obtained for each sample and the script written for their analysis

255 has been written in R (v4.2.2). The matrices have been analyzed using Seurat 4[46] using default
256 parameters. Each matrix has been filtered with the following cut-off: 500 < Features_RNA < 4000 ;
257 percent.mt < 5 and cells having two distinct TRA and TRB identified have been removed for the rest of
258 the analysis. Then each matrix has been normalized using the SCTransform method with a regression
259 on the percentage of ribosomal genes count. The four matrices has been merged and integrated using
260 harmony package[48]. The cell clusters have been identified using harmony for reduction. The markers
261 for each clusters has been identified with a min.pct=0.25 (genes detected in a minimum fraction of
262 min.pct cells) and a threshold of logFoldChange of 0.25. The markers retained for each clusters where
263 those having a p-value adjusted < 0.01. The annotation of clusters has been done using azimuth
264 package[46]. The module score has been calculated for each clusters using a predefined list of genes for
265 "Autoreactive", "Spike", "Flu" and "Calb". The top five percent of cells base on this module score has
266 been highlighted on the UMAP. The clusters have been then compared based on their module score
267 for each gene list using Kruskal Wallis test followed by a paired Wilcoxon rank test.

268 **Mini-bulk-RNA sequencing and analysis**

269 For mini-bulk RNA-seq of *in vitro* stimulated CD4 T cells, we used a slightly modified version of the
270 Flash-FB5P-seq protocol described above. First, CD4 T cell subsets were sorted on BD FACSAriaII. 500
271 to 2000 cells per well were stimulated in presence of 2.5µg/ml anti-CD3 and 1µg/ml anti-CD28. After
272 24h, cells were washed gently in PBS and resuspended in 4µL of specific lysis buffer with the
273 composition described above except for ERCC spike-in mix which we used 10-time more concentrated
274 (0.125 pg/µl). We performed RT-PCR with 16 µl of the RT-PCR mix described above, using 16 cycles of
275 PCR for cDNA amplification (instead of 22 cycles for single-cell assay). Sequencing libraries were
276 prepared and sequenced as described above for Flash-FB5P-seq. Sequencing reads were processed
277 with the zUMIs pipeline[42] to generate gene expression UMI count matrices. Mini-bulk gene expression
278 UMI count matrices were pooled across plates and further processed with the *DEseq2* package for
279 normalization (*vst* method) and computation of differentially expressed genes between non-
280 stimulated and TCR-stimulated cells from each sorted phenotype. The mean of normalized expression
281 values for manually selected significant DE genes was used to construct the heatmaps in Figure 5F.

282 **Bulk TCRβ sequencing**

283 $100x10^3$ PD-1^+CD45$RA^-$$CXCR5^-$ and PD-1^-CD45$RA^-$$CXCR5^-$ CD4 T cell subsets were sorted on a BD
284 FACSAriaII. gDNA from T cells and frozen liver biopsies was extracted with NucleoSpin® Blood kit
285 (Macherey-Nagel) and TCRβ sequencing was performed by Pr. Mascha Binder group (Halle, Germany).

286 **Unsupervised flow cytometry analysis**

287 Flow cytometry data from patients were analyzed using Omiq software (Dotmatics, USA). Subsampling
288 of viable lymphoid CD45RA- CD4+ CD3+ cells was performed ($20x10^3$ per patients). Clustering was
289 performed using FlowSOM to generate 150 clusters. 22 Metacluster were generated by running
290 consensus metaclustering. Wilcoxon test was used to identify significant variation between two groups
291 of patients.

292 **Spatial multi-phenotyping and analysis (Phenocycler instrument)**

293 The experiment was carried out according to the manufacturing instructions. Data are acquired as 3D
294 stacks by cycle of 4 markers (including a recurrent DAPI staining). The data are processed by computing
295 the more in focus image from the stack to take into account the potential tissue unflatness, every
296 cycles are registered together based on the DAPI staining, and the fluorescence signal is corrected by

297 background fluorescence based on blank cycles and normalized in intensity. Cell segmentation was
298 done by using Cellpose algorithm. After segmentation, measurement data are transformed in FCS files
299 and analyzed with the CODEX MAV software.

300 **Mice and treatments**

301 Heterozygous transthyretin (TTR)-inducible Cre (iCre) mice were back-crossed on a Balb/c background
302 for at least 10 generations (TAAM, CDTA CNRS Orléans, FRANCE). They were cross-bred with
303 homozygous Rosa26 hemagglutinin (HA) floxed mice resulting in heterozygous Rosa26 HA floxed (Ctrl)
304 mice and Rosa26 HA floxed TTR-inducible Cre (HA/iCre) mice. Mice were genotyped for Cre-coding
305 gene at 3 weeks-old thanks to small tail biopsies using following Cre primers: 5'-
306 CCTGGAAAATGCTTCTGTCCG-3' sense sequence and 5'-CAGGGTGTTATAAGCAATCCC-3' antisense
307 sequence. Male and female eight to twelve-weeks-old mice were used for each experiment. All mice
308 were housed at the UTE IRS-UN animal facilities (Nantes, FRANCE) where they were fed *ad libitum* and
309 allowed continuous access to tap water. Procedures were approved by the regional ethical committee
310 for animal care and use and by the Ministère de l'enseignement supérieur et de la recherche
311 (agreements APAFIS #2054, #28582 and #43529). All experiments were performed in accordance with
312 relevant guidelines and regulations.

313 Induction of HA expression by hepatocytes was performed by feeding mice with tamoxifen dry food
314 (0.5g/kg tamoxifen + 5% saccharose; Safe, FRANCE) for 14 days in free access or by injecting
315 intraperitonially (i.p) 1mg of tamoxifen diluted in corn oil three times in two weeks span. Peripheral
316 immunization against HA was performed with two different materials: one intramuscular (i.m)
317 injection of $1,5.10^9$ infectious particle of adenoviral CAG Cre vectors (AdCre, produced by INSERM UMR
318 1089 CPV facility, Nantes, FRANCE) in *tibialis anterior* of one posterior leg or i.m injection of 50µg of
319 plasmid CMV HA vector in *tibialis anterior* of both posterior legs, twice three weeks apart.

320 Immune checkpoint blockade protocol was performed by intravenous (i.v) injection of 200µg of anti-
321 mouse PD-1 antibody (29F.1A12™ clone, BioXCell) and 200µg of anti-mouse CTLA-4 antibody (9H10
322 clone, BioXCell), using purified Rat IgG2a,κ isotype control antibody (RTK2758 clone, Biolegend) and
323 polyclonal Syrian Hamster IgG antibody (ref BE0087, BioXCell) as controls, three times in one week
324 span. Depletion of $CD4^+$ cells was performed by i.p injection of 500µg of anti-mouse CD4 antibody
325 (GK1.5 clone, BioXCell), using purified Rat IgG2b,κ isotype control antibody (LTF-2 clone, BioXCell),
326 every two days during two weeks.

327 **RNA extraction, reverse transcription and quantitative PCR**

328 Total RNA was extracted from organ tissue using TRIzol™ reagent (15596026, ThermoFisher Scientific)
329 and purified with RNeasy Mini Kit (74106, Qiagen) according to the manufacturer protocol. Reverse
330 transcription was performed using 2µg of total RNA incubated at 70°C for 10min with poly-dT24
331 20µg/mL (Eurofins Genomics), 8mM DTT (18057018, ThermoFisher Scientific) and 20mM of each dNTP
332 (10297018, ThermoFisher Scientific). After a brief 5min incubation at 4°C, first strand buffer 5X
333 (Y00146, Invitrogen), 200U of M-MLV reverse transcriptase (18057018, ThermoFisher Scientific) and
334 40U of RNAse OUT inhibitor (10777019, Invitrogen) were added and incubated at 37°C for 1h followed
335 by 15min at 70°C. Real-time quantitative PCR was performed using the ViiA™ 7 Real-Time PCR System
336 and Power SYBR™ Green PCR Master Mix (4368708, ThermoFisher Scientific). Primers for HA (5'-
337 AAACTCTTCGCGGTCTTTCCA-3' sense sequence and 5'-GATAAGGTAGCTTGGGCTGC-3' antisense
338 sequence), Cre (see primers used for mice genotyping) and β-actine (5'-TACCACAGGCATTGTGATGG-3'

339 sense sequence and 5'-AATAGTGATGACCTGGCCGT-3' antisense sequence) were used. Relative HA
340 mRNA expression was determined with $2^{-\Delta\Delta CT}$ calculation, taking β-actine as reference gene and cDNA
341 from one conserved mouse that received i.v injection of AdCre (AdCre i.v) as positive control. Relative
342 Cre mRNA expression was determined with $2^{-\Delta CT}$ calculation, taking β-actine as reference gene.

343 **ELISA test**

344 Blood sample clotted for 1h at room temperature followed by centrifugation at 3000g for 10min and
345 serum was harvested and stored at -80°C. For detection of anti-HA antibodies, wells were coated with
346 1µg/mL of HA protein (11684-V08H, SinoBiological) diluted in coating buffer (Na_2CO_3 0.05M; $NaHCO_3$
347 0.05M; pH 9.2) and plate was incubated at 4°C overnight. Wells were washed and saturated with
348 dilution buffer (PBS 1X; Tween 20 0.05%; BSA 1%) for 2h at 37°C. Wells were washed, serum samples
349 were diluted by 500, 1000 and 5000 and added to wells in duplicate, and plate was incubated at 37°C
350 for 2h. Wells were washed and 0,4ng/mL of detection antibody (peroxidase-conjugated goat anti-
351 mouse IgG+IgM (H+L) polyclonal antibody, 115-036-068, Jackson ImmunoResearch) was added and
352 plate was incubated at 37°C for 1h. Finally, wells were washed and 50µL of TMB Substrate Reagent
353 (555214, BD Biosciences) was added for revelation step. Reaction was stopped 1min30sec after with
354 H_2SO_4 0.5M. Optical density (OD) at 450nm and 620nm were determined using a Spark® 10M Infinite
355 M200 Pro plate reader (TECAN). Analysis was performed by subtract OD_{620nm} to OD_{450nm} value, calculate
356 the mean of each duplicate and subtract the mean of blank wells to the mean of samples. Then, OD
357 values of each dilution of sample were normalized to OD values of each corresponding dilution of
358 positive control serum sample from one conserved AdCre i.v mouse. Finally, for each sample, mean of
359 normalized OD_{450nm} for each dilution was calculated and analyzed.

360 **Cell preparation, tetramer enrichment and staining and flow cytometry**

361 Splenocytes were isolated by mechanical dissociation of spleen in red blood cell lysis buffer (NH_4Cl
362 155mM; $KHCO_3$ 10mM; EDTA 1mM; Tris 17mM per 1L of sterilized water). Liver non-parenchymal cells
363 (NPCs) were isolated as previously described (Le Guen et al., 2017) from liver sample perfused with
364 HBSS 1X. Briefly, livers were digested with collagenase IV, then NPCs were enriched by Percoll density
365 gradient centrifugation and red blood cells lysis. 20.10^6 splenocytes and 3.10^6 NPCs were stained with
366 both I-A^d-HA peptide (HNTNGVTAACSHE) and I-E^d-HA peptide (SFERFEIFPKE) PE-labelled tetramers
367 (NIH Tetramer Core Facility; Atlanta, USA) at room temperature during 1h. Cells were washed and
368 stained with magnetic anti-PE microbeads (130-048-801, Miltenyi) at 4°C during 15min. Cells were
369 washed and enriched using magnetic MS columns (130-042-201, Miltenyi). Positive fraction was kept
370 for HA-specific $CD4^+$ T cell detection. Negative fraction was stained with H-$2K^d$-HA peptide
371 (PEYWEEQTQRAKSD) PE-labelled tetramer (NIH Tetramer Core Facility; Atlanta, USA) at room
372 temperature during 1h for HA-specific $CD8^+$ T cell detection. All cells were washed and viability staining
373 (LIVE/DEAD™ Fixable Aqua Dead Cell Stain kit, L34957, ThermoFisher Scientific) was performed at 4°C
374 during 15min, protected from light. Cells were washed and extracellular staining were performed at
375 4°C during 20min protected from light, using fluorochrome-coupled anti-mouse antibodies
376 (Supplementary table 1). Fluorescence was measured on BD FACSCantoII or BD FACSAriaII (BD
377 Biosciences; Mountain View, USA). HA-specific memory CD4 (or CD8) T lymphocytes were defined as:
378 LIVE/$DEAD^-$ $CD19^-$ $CD4^+$ (or $CD8^+$) $CD44^{high}$ $tetramer^+$ cells. FlowJo software (TreeStar Inc) was used to
379 analyze flow cytometry data.

380 **3'-end bulk RNA sequencing**

381 50 up to 200 HA-specific memory $CD4^+$ T cells were FACS sorted. RNA extraction, reverse transcription
382 and PCR steps were directly performed after sorting according to the SMART-Seq® v4 Ultra® Low Input
383 RNA Kit protocol (Takara Bio, USA). Amplified complementary DNA were transferred to the Benaroya
384 Research Institute (Seattle, USA) to perform a 3'-end bulk RNA sequencing. To normalize, trimmed-
385 mean of M values (TMM) normalization on the raw gene counts was performed. Additionally, because
386 many genes are not expressed in any of the samples and are therefore uninformative, a filtering step
387 was performed requiring that genes are expressed with at least 1 count per million total reads in at
388 least 10% of the total number of libraries. For the differential gene expression analysis, we used the
389 following threshold: fold change (FC) > 2 and adjusted p value < 0.1.

390 **Histological analysis**

391 Liver lobes were fixed in formol 4% (VWR) for 24h at room temperature. Dehydration in differential
392 absolute ethanol baths, embedding in paraffin and staining of paraffin-embedded sections (3µm) with
393 hematoxylin-phloxin-saffron (HPS) coloration were performed by the IBISA MicroPICell facility
394 (Biogenouest; Nantes, FRANCE). Slides were scanned and observed using NanoZoomer (Hamamatsu)
395 and NDP Scan software. Histological analysis was performed thanks to a liver inflammation scoring
396 method based on established hepatitis grading[50], simplified to portal inflammation score (0 to 4),
397 lobular inflammation score (0 to 4) and presence of interface hepatitis (0 to 1), giving a minimum score
398 of 0 and maximum score of 9. Liver inflammation scoring was performed blindly.

399 **Western blot**

400 Total proteins were extracted from liver samples via RIPA buffer treatment. 25µg of protein were
401 denatured at 95°C for 5min in Laemmli Sample Buffer (161747, Bio-Rad) with DTT 0.1M. Preparation
402 was separated by SDS-PAGE on Mini-PROTEAN TGX Precast Protein Gels (4561036, Bio-Rad) in
403 migration buffer (Tris 15g/L; Glycine 72g/L; SDS 10g/L) and transferred onto a PVDF membrane with
404 the Trans-Blot Turbo Transfer System (Bio-Rad). The membrane was blocked for 2h with a blocking
405 solution (TBS; Tween 20 0.1%; Skim milk 5%), followed by overnight incubation at 4°C with anti-HA
406 antibody (rabbit polyclonal antibody; 11684-T62, Sinobiological) and anti-mouse β-actin antibody
407 (mouse monoclonal antibody; 3700, Cell Signaling) as primary antibodies. The membrane was washed
408 and incubated 1h at room temperature with peroxidase-conjugated donkey anti-rabbit IgG (H+L)
409 antibody (E-AB-1080-120, Cliniscience) and peroxidase-conjugated goat anti-mouse IgG+IgM (H+L)
410 antibody (115-036-068, Jackson ImmunoResearch). Revelation was performed by
411 Electrochemioluminescence Super Signal West Pico (34577, ThermoFisher Scientific) according to the
412 manufacturer instructions. Imaging and analysis of western blots were performed on the ChemiDoc
413 MP Imaging System (Bio-Rad).

414 **Statistical analysis**

415 Statistical comparisons were performed using GraphPad Prism software V.5 (GraphPad Software, La
416 Jolla, CA, USA) and FaDA (https://shiny-bird.univ-nantes.fr/app/Fada). P value <0.05 after adjustment
417 were considered significant.

Name	Clone	Antigen	Brand	Reactivity	Application
APC/Cyanine7 anti-human CD69	FN50	CD69	BioLegend	Human	Flowcytometry
Alexa Fluor®647 anti-human CD185 (CXCR5)	J252D4	CD185	BioLegend	Human	Flowcytometry
PerCP/Cyanine5.5 anti-human CD279 (PD-1)	EH12.2H7	CD279	BioLegend	Human	Flowcytometry

Alexa Fluor® 488 anti-human CD4	OKT4	CD4	BioLegend	Human	Flowcytometry
APC/Cyanine7 anti-human CD4	RPA-T4	CD4	BioLegend	Human	Flowcytometry
Alexa Fluor®647 anti-human CD25	BC96	CD25	Invitrogen	Human	Flowcytometry
PerCP/Cyanine5.5 anti-human HLA-DR	G46-6	HLA-DR	BD Biosciences	Human	Flowcytometry
Alexa Fluor® 488 anti-human CD185 (CXCR5)	RF8B2	CD185	BD Biosciences	Human	Flowcytometry
Brilliant Violet 421™ anti-human CD45RA	HI100	CD45RA	BioLegend	Human	Flowcytometry
APC anti-human CD184 (CXCR4)	12G5	CD184	BioLegend	Human	Flowcytometry
Brilliant Violet 421™ anti-human CD278 (ICOS)	C398.4A	CD278	BioLegend	Human	Flowcytometry
Brilliant Violet 605™ anti-human CD200 (OX2)	OX-104	CD200	BioLegend	Human	Flowcytometry
Brilliant Violet 650™ anti-human CD183 (CXCR3)	G025H7	CD183	BioLegend	Human	Flowcytometry
Brilliant Violet 711™ anti-human CD196 (CCR6)	G034E3	CD196	BioLegend	Human	Flowcytometry
Brilliant Violet 750™ anti-human CD185 (CXCR5)	J252D4	CD185	BioLegend	Human	Flowcytometry
Brilliant Violet 785™ anti-human CD49d	9F10	CD49d	BioLegend	Human	Flowcytometry
FITC anti-human CD57	HNK-1	CD57	BioLegend	Human	Flowcytometry
PE/Cyanine5 anti-human HLA-DR	L243	HLA-DR	BioLegend	Human	Flowcytometry
PE/Fire™ 700 anti-human CD25	M-A251	CD25	BioLegend	Human	Flowcytometry
PerCP/Cyanine5.5 anti-human CD27	M-T271	CD27	BioLegend	Human	Flowcytometry
Alexa Fluor® 700 anti-human CD127 (IL-7Rα)	A019D5	CD127	BioLegend	Human	Flowcytometry
APC/Fire™ 810 anti-human CD38	HIT2	CD38	BioLegend	Human	Flowcytometry
BD OptiBuild™ BUV395 Mouse Anti-Human CD45RA	5H9	CD45RA	BD Biosciences	Human	Flowcytometry
BD Horizon™ BUV496 Mouse Anti-Human CD16	3G8	CD16	BD Biosciences	Human	Flowcytometry
BD Horizon™ BUV737 Mouse Anti-Human CD56	NCAM16.2	CD56	BD Biosciences	Human	Flowcytometry
BD Horizon™ BUV805 Mouse Anti-Human CD8	SK1	CD8	BD Biosciences	Human	Flowcytometry
Brilliant Violet 510™ anti-human CD3	OKT3	CD3	BioLegend	Human	Flowcytometry
Pacific Blue™ anti-human CD161	HP-3G10	CD161	BioLegend	Human	Flowcytometry
PE anti-human TIGIT (VSTM3)	A15153G	TIGIT	BioLegend	Human	Flowcytometry
PE/Cyanine7 anti-human CD279 (PD-1)	EH12.2H7	CD279	BioLegend	Human	Flowcytometry
Spark Blue™ 550 anti-human CD4	SK3	CD4	BioLegend	Human	Flowcytometry
APC/Fire™ 750 anti-human/mouse Granzyme B	QA16A02	Granzyme B	BioLegend	Human	Flowcytometry
Brilliant Violet 605™ anti-human HLA-DR	L243	HLA-DR	BioLegend	Human	Flowcytometry
Brilliant Violet 650™ anti-human CD28	CD28.2	CD28	BioLegend	Human	Flowcytometry
Brilliant Violet 711™ anti-human CD39	A1	CD39	BioLegend	Human	Flowcytometry
BD OptiBuild™ BV750 Mouse Anti-Human TCR Vα7.2	OF-5A12	TCR Vα7.2	BD Biosciences	Human	Flowcytometry
Brilliant Violet 785™ anti-human CD27	O323	CD27	BioLegend	Human	Flowcytometry
BD Horizon™ PE-CF594 Mouse Anti-EOMES	X4-83	EOMES	BD Biosciences	Human	Flowcytometry
PerCP/Cyanine5.5 anti-human Granzyme A	CB9	Granzyme A	BioLegend	Human	Flowcytometry
Spark NIR™ 685 anti-human FOXP3	206D	FOXP3	BioLegend	Human	Flowcytometry
Anti-Hu CD20-BX007—Alexa Fluor™ 750	L26	CD20	Akoya	Human	Phenocycler
Anti-Hu CD31-BX001—Alexa Fluor™ 750	EP3095	CD31	Akoya	Human	Phenocycler
Anti-Hu Pan-Cytokeratin-BX019—Alexa Fluor™ 750	AE1-AE3	PANCK	Akoya	Human	Phenocycler
Anti-Hu CD8-BX026—Atto 550	C8/144B	CD8	Akoya	Human	Phenocycler
Anti-Hu CD21-BX032—Atto 550	EP3093	CD21	Akoya	Human	Phenocycler
Anti-Hu CD38-BX089—Atto 550	AKYP0110	CD38	Akoya	Human	Phenocycler
Anti-Hu IFNG-BX020—Atto 550	AKYP0093	IFNG	Akoya	Human	Phenocycler
Anti-Hu PD-1-BX046—Cy5	NAT105	PD1	Akoya	Human	Phenocycler
Anti-Hu ICOS-BX054—Cy5	SP98	ICOS	Akoya	Human	Phenocycler
Anti-Hu CD4-BX003—Cy5	EPR6855	CD4	Akoya	Human	Phenocycler
Anti-Hu CD3-BX003—Cy5	EP449E	CD3	Akoya	Human	Phenocycler

Anti-Hu CXCR5-BX042—Cy5	EPR23463-30	CXCR5	Abcam	Human	Phenocycler
PerCP/Cyanine5.5 anti-mouse CD4	RM4-5	CD4	BD Biosciences	Mouse	Flowcytometry
FITC anti-mouse CD4	GK1.5	CD4	BioLegend	Mouse	Flowcytometry
FITC anti-mouse CD8a	53-6.7	CD8	BD Biosciences	Mouse	Flowcytometry
APC anti-mouse CD44	IM7	CD44	BioLegend	Mouse	Flowcytometry
APC/Cyanine7 anti-mouse CD44	IM7	CD44	BioLegend	Mouse	Flowcytometry
Brilliant Violet 421™ anti-mouse CD279 (PD-1)	J43	CD279	BioLegend	Mouse	Flowcytometry
APC anti-mouse TIGIT	4D4	TIGIT	BioLegend	Mouse	Flowcytometry
Brilliant Violet 510™ anti-mouse CD19	1D3	CD19	BioLegend	Mouse	Flowcytometry

Supplementary Table1. Antibody listing

Results.

- **Self-antigens-specific CD4 T cell detection in AILD patients with auto-antibodies.**

We have previously shown that Sepsecs (SLA)-specific CD4 T cells are detectable in the blood of patients with autoimmune hepatitis (AIH) whose serum contains anti-SLA antibodies[22]. In the present study, we investigated whether we could extend those findings to autoreactive CD4 T cells specific for other antigens frequently targeted by autoantibodies in AILD. We studied the reactivity of CD4 T cells against Sepsecs (targeted by anti-SLA autoantibody), CYP2D6 (targeted by anti-LKM1 autoantibody) and PDCE2 (target by anti-M2 autoantibody) in AILD (AIH, PBC and overlap AIH/PBC) patients with or without anti-SLA (SLA+) or anti-LKM1 (LKM1+) or anti-M2 (M2+) autoantibodies. As an experimental control, we also studied the reactivity of CD4 T cells against MP65 (Candida Albicans; C.ALB), MP1 (Influenza; H1N1) and SPIKE (SARS-Cov2) in the AILD patients. As previously described, detection of antigen-specific CD4 T cells was achieved after brief peptide stimulation *in vitro*. CD4 T cells that specifically recognize antigen-derived peptides upregulate CD40 ligand (CD154) and can be detected by flow cytometry (Figure 1A and B). These reactive CD4 T cells were memory cells (CD45RA-; mCD4 T cells) expressing high levels of PD1 but not CXCR5 (Figure 1B and C). The frequency of Sepsecs-, CYP2D6- and PDCE2-specific PD1+ CXCR5- mCD4 T cells was only detectable and significantly higher in patients with the presence of specific autoantibodies in the blood of patients (Figure 1D). In comparison, the frequency of MP1 (H1N1)-, MP65 (C.ALB)- and SPIKE (SARS-Cov2)-specific CD4 T cells was high in the blood of all patients (Figure 1E). Foreign antigen-specific CD4 T cells were also mCD4 T cells. MP1- and SPIKE-specific CD4 T cells, expressed PD1. Neither MP1-, MP65- and SPIKE-specific CD4 T cells expressed significant levels of CXCR5 (Figure 1E). In conclusion, during AILD, we observed a correlation between the specific autoimmune humoral response and the presence of circulating self-antigen specific CD4 T cells.

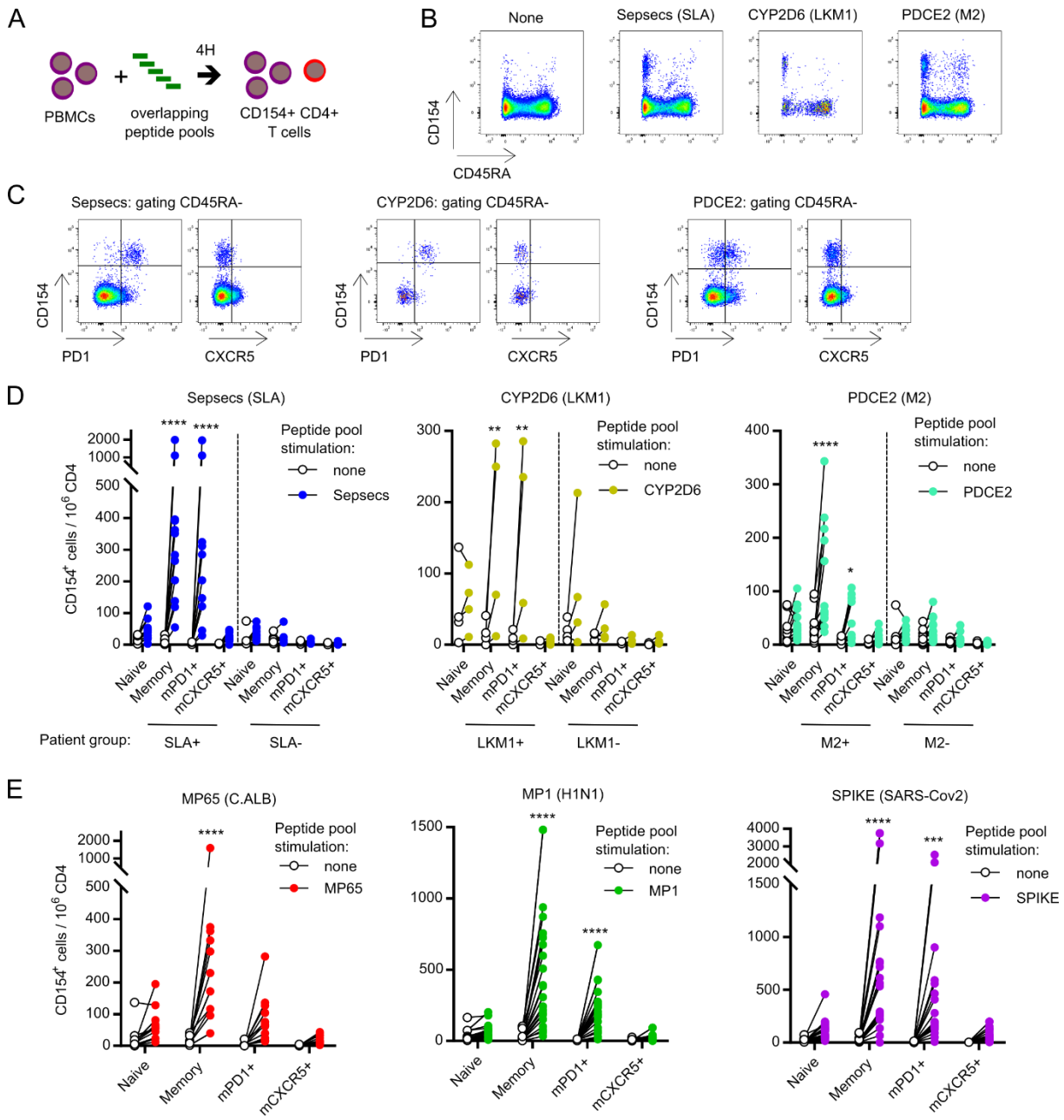

Figure 1. Detection and immune-phenotyping of circulating liver-self-antigen-specific CD4 T cells. (A) Schematic representation of the detection of antigen-specific CD4 T cells based on the upregulation of CD40 ligand (CD154) after 4 hours of *ex vivo* peptide stimulation. (B) Pseudocolor dot plot representation of CD45RA and CD154 expression at the surface of CD4 T cells after stimulation with peptide pools from the indicated antigens. (C) Pseudocolor dot plot representation of PD1, CXCR5 and CD154 expression at the surface of CD45RA- mCD4 T cells after stimulation with peptide pools from the indicated antigens. (D) Frequency of CD154+ naïve, memory, memory PD1+ (mPD1+) and memory CXCR5+ (mCXCR5+) CD4 T cells per million CD4 T cells after Sepsecs, CYP2D6 or PDCE2 peptides stimulation of PBMCs from 12 SLA+ patients and 9 SLA- patients (left); or 4 LKM1+ patients and 4 LKM1- patients (central); or 14 M2+ patients and 14 M2- patients (right). (E) Frequency of CD154+ naïve, memory, mPD1+ and mCXCR5+ CD4 T cell per million CD4 T cells after MP65 (C.ALB), MP1 (H1N1) or SPIKE (SARS-Cov2) peptides stimulation of PBMCs from 13, 24 and 23 patients respectively. Sidak's multiple comparisons test was used for D and E. *: p<0.05; **: p<0.01; ***: p<0.001; ****: p<0.0001.

- **Self-antigens-specific CD4 T cells have a unique transcriptomic immune signature during AILD.**

We sorted self-antigen-specific and foreign antigen-specific mCD4 T cells by flow cytometry for single-cell RNA-seq and TCR-seq analyses (Figure 2). An unsupervised clustering analysis led to the

identification of eight clusters (Figure 2A). The majority of transcriptional clusters corresponded to distinct antigenic specificities rather than to distinct patients: e.g. most of the MP65-specific CD4 T cells gathered in cluster 5 (Figure 2B and C). The only notable exception was cluster 7, which corresponded to a PDCE2-specific CD4 T cell clonotype from one patient (01-176) with a unique cytotoxic profile (Supplementary Figure 1). As the memory response against an antigen is generally associated with clonal expansion, we analyzed the diversity and proportion of clonotypes for each antigen reactivity (Figure 2D). Clonal expansion was observed for every antigenic reactivity, whether associated with self- or foreign-reactivity. Analysis of these expanded clones for cluster affiliation demonstrated that transcriptional clusters were linked to antigenic reactivity, meaning that CD4 T cell antigenic reactivity was associated with a distinct transcriptomic signature (Figure 2E). Interestingly, all three liver auto-reactivities were grouped in the same clusters. MP1-specific CD4 T cells were in the cluster 0; MP65-specific CD4 T cells were in the cluster 5; SPIKE-specific CD4 T cells were in the cluster 6 and Sepsecs-, CYP2D6- and PDCE2-specific CD4 T cells were in the clusters 2 and 3. Two clusters (4 and 1) were not linked to antigenic reactivity. We annotated four antigen-reactivity groups based on unsupervised transcriptional clustering: the H1N1 cluster, containing MP1-specific CD4 T cells (cluster 0); the C.ALB cluster, containing MP65-specific CD4 T cells (cluster 5); the SARS-Cov2 cluster, containing SPIKE-specific CD4 T cells (6); and the auto-reactivity cluster, containing Sepsecs-, CYP2D6- and PDCE2-specific CD4 T cells (clusters 2 and 3) (Figure 2F and G). The transcriptional signature of self-antigen-specific CD4 T cells (auto-reactivity) was clearly distinct from that of the three foreign antigen-reactivity groups. The gene signature of autoantigen-reactive cells was linked to the regulation of T cell activation and immune exhaustion (*CTLA4, TIGIT, BATF, IL21, CD74, PRDM1, TOX*). This gene signature, together with the *CXCL13* gene, was also linked to the B-helper autoreactive signature of T peripheral helper cells (TPH) described in other autoimmune disorders (Figure 2H). In comparison, the H1N1 gene signature was associated with a classical antiviral response and T cell chemotaxis (*GZMB*, *CCL4, CCL5 and FASLG*). The Candida Albicans gene signature was associated with a type 17 helper and defense response (*CCL20, IL22, IL17A, IL23A*). SARS-CoV2 gene signature was associated with a type 2 helper response and B cell activation (*TNFRSF4, CCR4, IL4 and IL13*). We had the opportunity to longitudinally analyze the TCR clonotypes of Sepsecs-specific and MP65-specific CD4 T cells of patients (n=3 and 1, respectively) over 3 years (2018 to 2021). Although variable numbers of novel clones were detected in patients' blood over time, some conserved Sepsecs-specific CD4 T clonotypes were detected over the 3-year period (Supplementary Figure 2), suggesting chronically active clonal expansion of autoreactive CD4 T cells despite their immuno-exhausted molecular profile (expression of *CTLA4, TIGIT* and other markers as described earlier). Altogether, these data demonstrate that distinct liver-self-antigen-specific CD4 T cells had a common specific B-helper autoreactive signature, with high-level expression of checkpoint inhibitors (immuno-exhausted transcriptional profile).

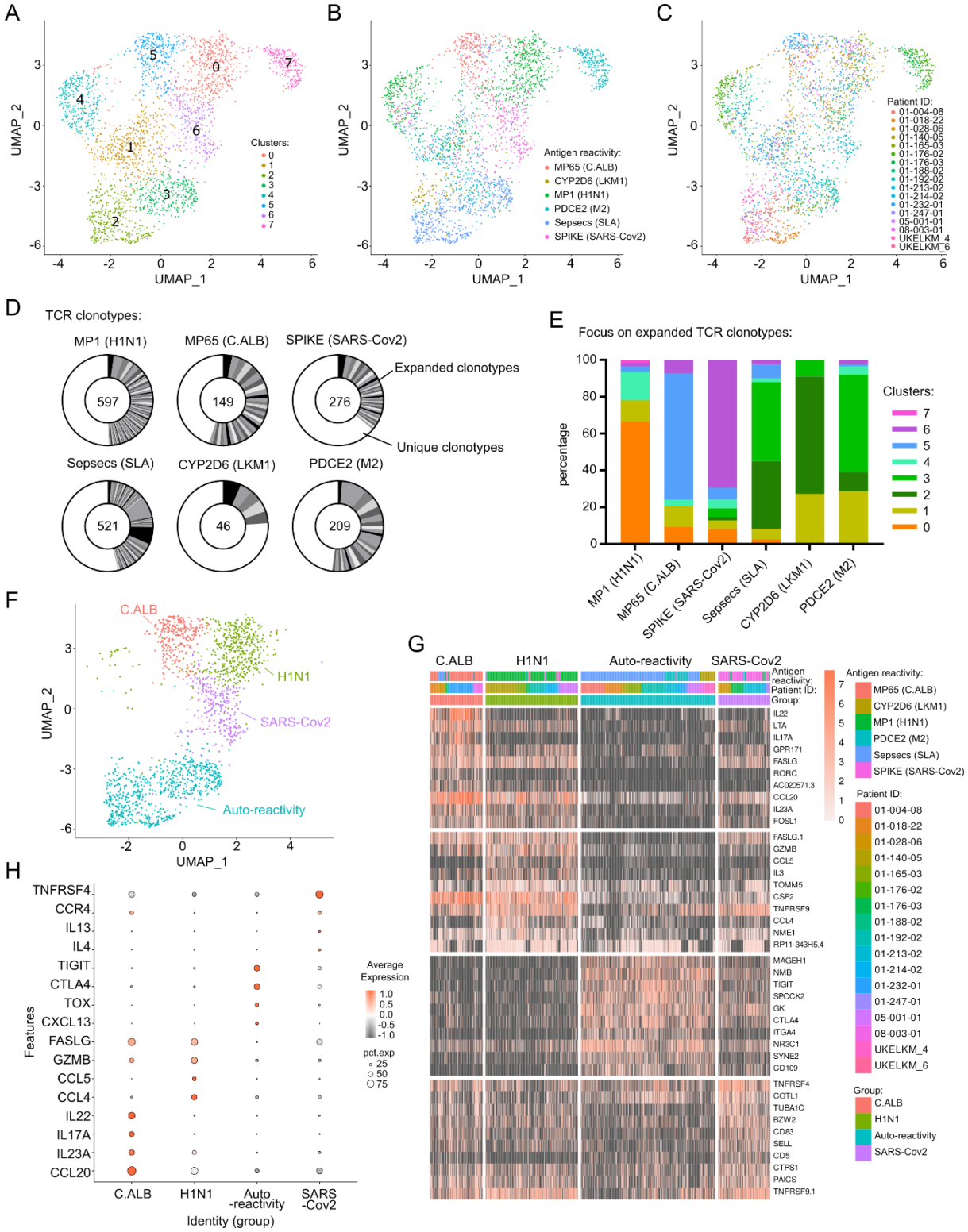

Figure 2. Single-cell RNA sequencing of liver-self-antigens specific CD4 T cells. A total of 2768 CD154+ mCD4 T cells (648 Sepsecs-, 113 CYP2D6-, 583 PDCE2-, 273 MP65-, 798 MP1- and 353 SPIKE-specific CD4 T cells) from 7 SLA+, 3 LKM1+ and 6 M2+ patients were analyzed for transcriptome and TCR sequences at the single cell level using FB5P-seq. (A) UMAP representation of antigen-specific memory CD4 T cell single-cell transcriptomes, colored by non-supervised Louvain cluster identity. (B) UMAP representation colored by antigen reactivity. (C) UMAP representation colored by patient ID. (D) TCRαβ clonal diversity of antigen-specific single T cells for each antigen- reactivity. Numbers indicate the number of single cells analyzed with a TCRαβ sequence. Black and grey sectors indicate the proportion of TCRαβ clones (clonotype common to ≥ 2 cells) within single-cells analyzed; white sector: unique clonotypes. (E) Louvain cluster distribution of antigen-specific T cell clonotypes for each reactivity, as indicated. (F) UMAP representation of selected antigen reactivity cluster groups of memory

503 CD4 T cells (C.ALB, H1N1, SARS-Cov2 and auto-reactivity). (G) Single-cell gene expression heatmap for top 10 marker genes
504 of cells from each antigen reactivity group defined in (F). (H) Dot plot representation of four selected marker genes of clusters
505 C.ALB, H1N1, SARS-Cov2 and auto-reactivity.

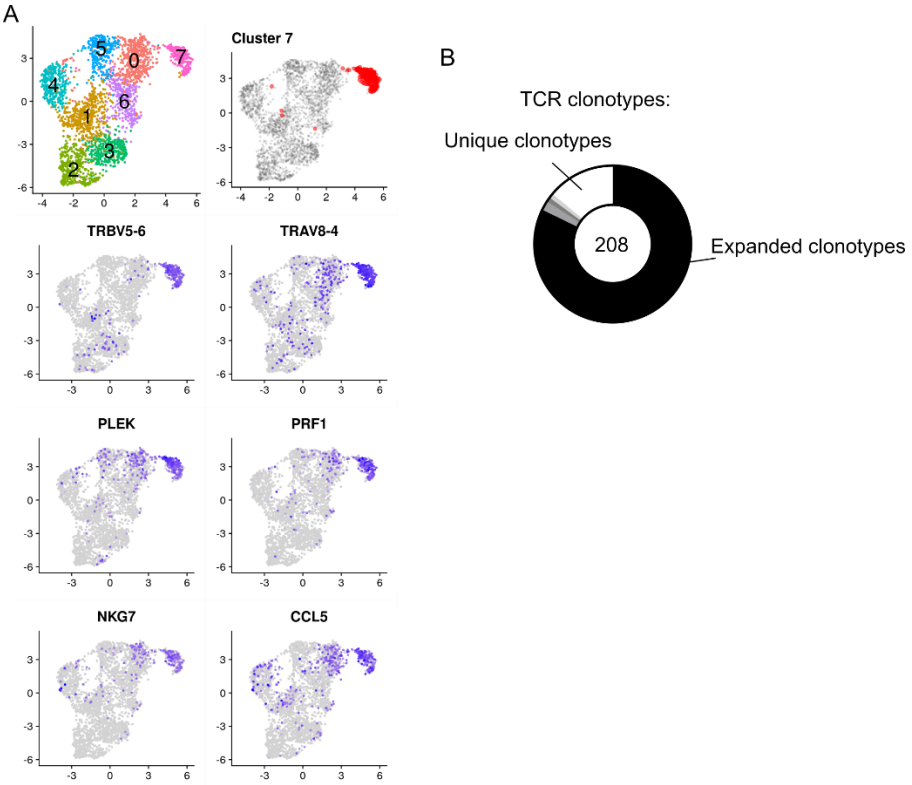

506

507 **Supplementary figure 1: Characterization of the cluster 7 of PDCE2-specific CD4 T cells.** (A) UMAP representation of selected
508 gene markers. (B) TCRαβ clonal diversity of antigen-specific single T cells for cluster 7 cells. Numbers indicate the number of
509 single cells analyzed with a TCRαβ sequence. Black and grey sectors indicate the proportion of TCRαβ clones (clonotype
510 common to ≥ 2 cells) within single-cells analyzed; white sector: unique clonotypes.

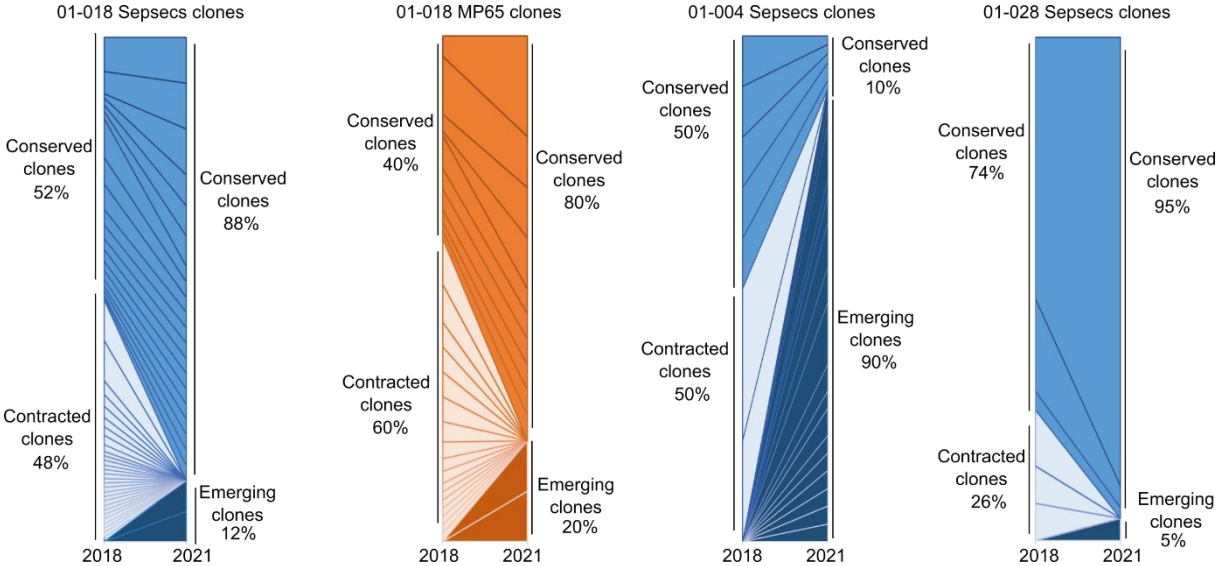

511

512 **Supplementary figure 2: Longitudinal analysis of Sepsecs-specific clonotypes.** Representation of the proportion of Sepsecs-
513 and MP65-clonotypes between 2018 and 2021 in the blood of three patients.

514 - **Clonal overlap between circulating autoreactive and intra-hepatic CD4 T cells in AILD.**

515 We then attempted to answer the following question: how related to liver infiltrating CD4 T cells are
516 circulating autoreactive CD4 T cells in AILD? We hypothesized that the specific molecular profile of
517 circulating autoreactive CD4 T cells was induced during chronic antigen reactivity in the tissue. Thus, it
518 is possible that mCD4 T cells activated *in situ* in autoimmune lesions in the liver would proliferate and
519 that circulating self-antigen-reactive CD4 T cells may represent clonal relatives of those liver CD4 T
520 cells. We set out to track T cell clonotypes from blood CD4 T cell samples in matching liver biopsies,
521 and to analyze the immune phenotype of circulating CD4 T cells with matched TCR clonotype. For one
522 SLA+ patient analyzed by peptide restimulation and single-cell sequencing (Figure 2, patient 01-192),
523 we also had access to a frozen liver biopsy, from which we derived bulk TCR-beta-seq data
524 (Supplementary Figure 3A). Six out of sixty (10%) Sepsecs-specific circulating CD4 TCR clonotypes were
525 also detected in the liver, compared to only one out of forty-six (2.2%) MP1-specific TCR clonotypes
526 (H1N1). Bulk TCR-beta sequence counts corresponding to Sepsecs-specific clonotypes suggested few
527 clonal expansions dominating the Sepsec-specific response also in the liver (Supplementary Figure 3C).
528 Thus, for this patient, circulating self-antigen-specific CD4 T cells accurately reflected clonally
529 expanding autoantigen-specific T cells within the liver.

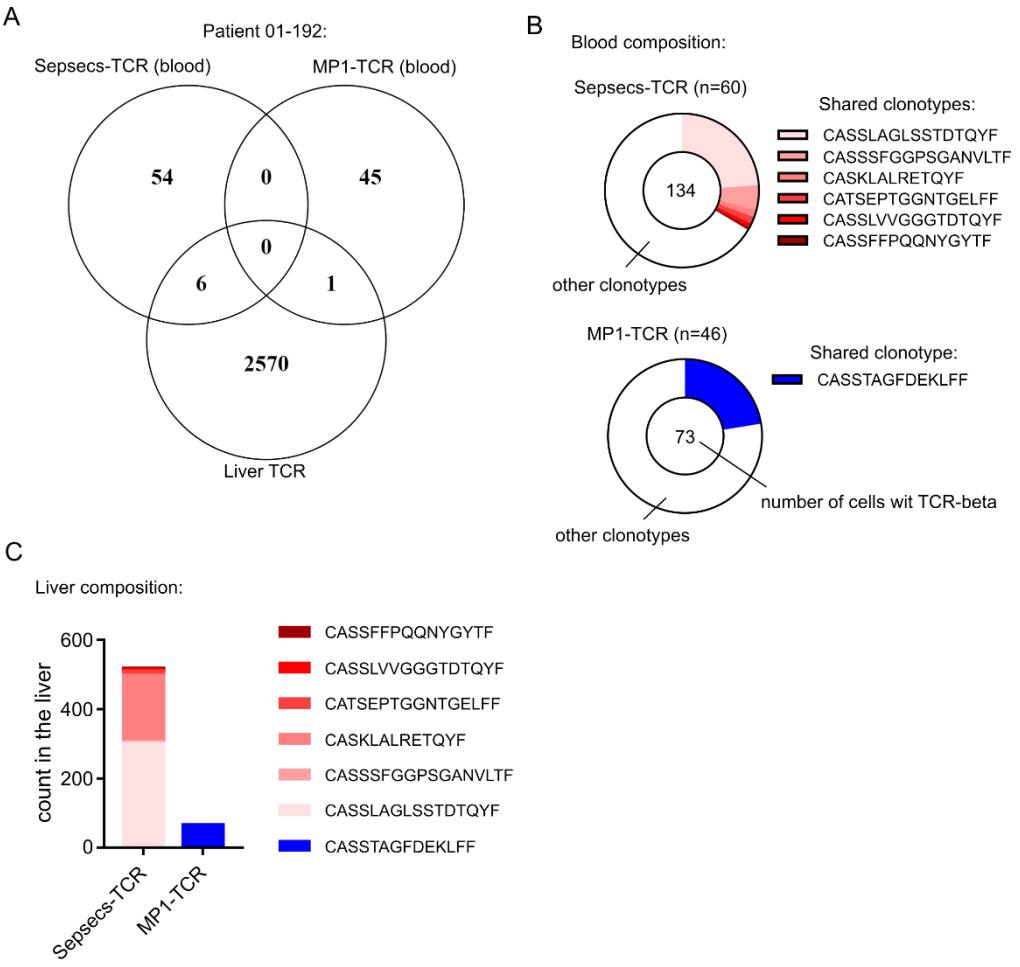

530

531 **Supplementary figure 3: Sepsecs-clonotypes are enriched in the liver of an SLA+ patient.** (A) Shared TCR between Sepsecs-
532 specific CD4 T cells, MP1-specific CD4 T cells and the liver biopsy. (B) Proportion of shared TCR with the liver (colored sectors)
533 within TCRαβ clonal diversity of Sepsecs- or MP1-specific CD4 T cells. (C) Liver frequency (count) of shared-TCRβ sequences.

534 For most AILD patients, no self-antigen reactivity is known, therefore, to continue exploring the
535 relationship between circulating and liver CD4 T cells, we took advantage of our initial observation that
536 in AILD, most circulating self-antigen-specific CD4 T cells have a PD1+ CXCR5- CD45RA- memory
537 phenotype[22] (Figure 1). We had access to paired blood-liver samples from 4 AILD patients; for each,

538 we extracted genomic DNA and performed bulk TCR-beta-seq from blood PD1+ CXCR5- mCD4 T cells,
539 blood PD1- mCD4 T cells, and whole liver biopsy (Supplementary Figure 4A). First, we observed that
540 the 100 most abundant TCR-beta sequences in the liver account for more than 50% of intrahepatic
541 TCRs, suggesting strong local clonal expansion (Supplementary Figure 4B). We also observed that the
542 PD1+ CXCR5- mCD4 T cell population shared more TCR-beta sequences with the liver than PD1- mCD4
543 T cells (Supplementary Figure 4C). Interestingly, the proportion of TCR-beta sequences from the PD1+
544 CXCR5- mCD4 T cell population, which were among the top 100 TCR-beta sequences in the liver, was
545 more important than those from PD1- mCD4 T cells (supplementary Figure 4D). This data
546 demonstrated the circulating PD1+ CXCR5- mCD4 T cell population contain dominant intrahepatic CD4
547 T cell clonotypes in comparison to the PD1- mCD4 T cell population.

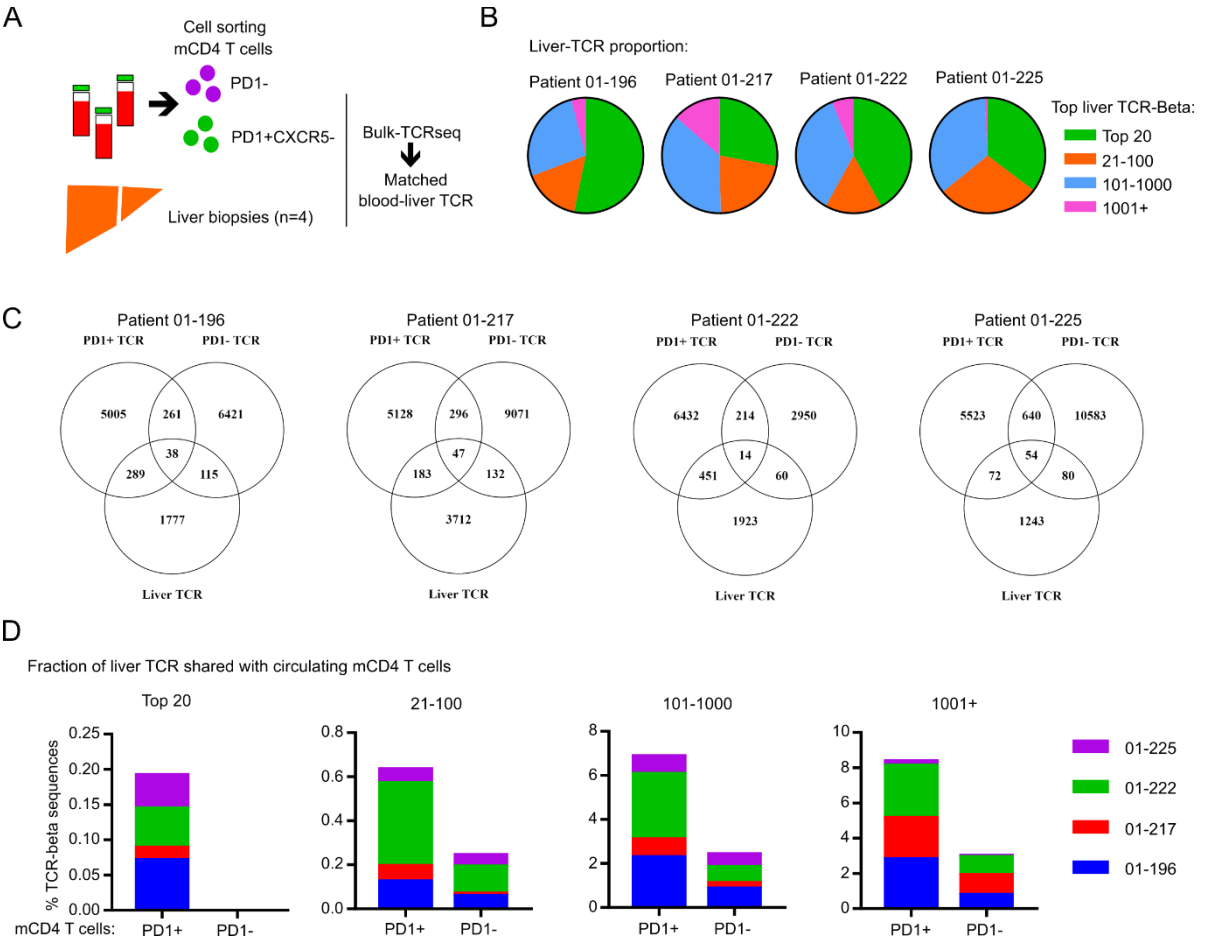

548

549 **Supplementary figure 4: Shared TCRβ sequences between Blood PD1+ or PD1- CD4 T cells and the liver biopsies from four**
550 **distinct patients**. (A) Experimental design for bulk TCRβ sequencing. (B) Pie chart showing the proportion of the TCRβ
551 repertoire occupied by the top 20, 100, 1000 or 1001+ clones. (C) Shared TCRβ sequences between Blood PD1+ or PD1- mCD4
552 T cells and the liver biopsies from the four distinct patients. (D) Analysis of the percentage of TCRβ clonotypes shared between
553 the top 20, 100, 1000 or 1001+ liver clones and the circulating PD1+ CXCR5- (PD1+) or PD1- mCD4 T cells (PD1-) from four
554 distinct AILD patients.

555 Based on this, we performed droplet-based single-cell RNA-seq combined with TCR sequencing of
556 blood PD1+ CXCR5- mCD4 T cells from four patients to characterize the transcriptional profile of cells
557 with TCR clonotypes detected in the matched liver biopsies (Figure 3A). First, cluster analysis of PD1+
558 CXCR5- mCD4 T cells revealed the heterogeneity of these cells (Figure 3B). The main subsets identified
559 by unsupervised azimuth annotation and marker gene analysis were: *GZMK*+ effector CD4 T cells (TEM
560 GZMK+, cluster 1); *HLA-DR*+ central memory CD4 T cell (TCM HLA-DR+, cluster 2), *NKG7*+ effector CD4
561 T cell (TEM NKG7+, clusters 3); cytotoxic (*GZMB*+*GNLY*+) CD4 T cells (CTL, clusters 5) and *FOXP3*+

562 (regulatory) CD4 T cell (Treg, cluster 6) (Figure 3B and C, and supplementary Figure 5 and 6). Clusters
563 4, 7 and 8 were likely subsets of TCM but were difficult to further annotate based on marker genes.

564 In this data set, we analyzed the TCR-beta sequences found in the top 100 TCR-Beta sequences in the
565 liver (Figure 3D). For each of these liver TCR-beta clones, we assigned a cluster identification based on
566 single-cell transcriptomic data from PD1+ CXCR5- mCD4 T cells (Figure 3D). The analysis revealed top
567 expanded intrahepatic clones found in the blood were mainly distributed between cluster 1 (TEM
568 GZMK+), cluster 2 (TCM HLA-DR+) and cluster 3 (TEM NKG7+). We computed gene set scores based on
569 our analyses of peptide-stimulated T cells (Figure 2), with the expression of the top 50 genes
570 (avg_log2FC) from self-antigens (auto-reactivity)- or H1N1 MP1-specific CD4 T cells, respectively. These
571 scores were then quantified in the droplet-based scRNA-seq dataset of non-stimulated PD1+ CXCR5-
572 mCD4 T cells (Figure 3E). Cells in cluster 2 (TCM HLA-DR+) had the highest score for the auto-reactivity
573 module, while cells in clusters 3 and 5 had the highest score for the H1N1 module. These data suggest
574 that cells in cluster 2, PD1+ CXCR5- HLA-DR+ central memory CD4 T cells (TCM HLA-DR+), were the
575 main circulating CD4 T cell clonal counterpart of liver-autoreactive CD4 T cells. Interestingly, this cluster
576 2 also contained proliferative CD4 T cells, reinforcing the idea of local clonal expansion.
577 (Supplementary figure 6).

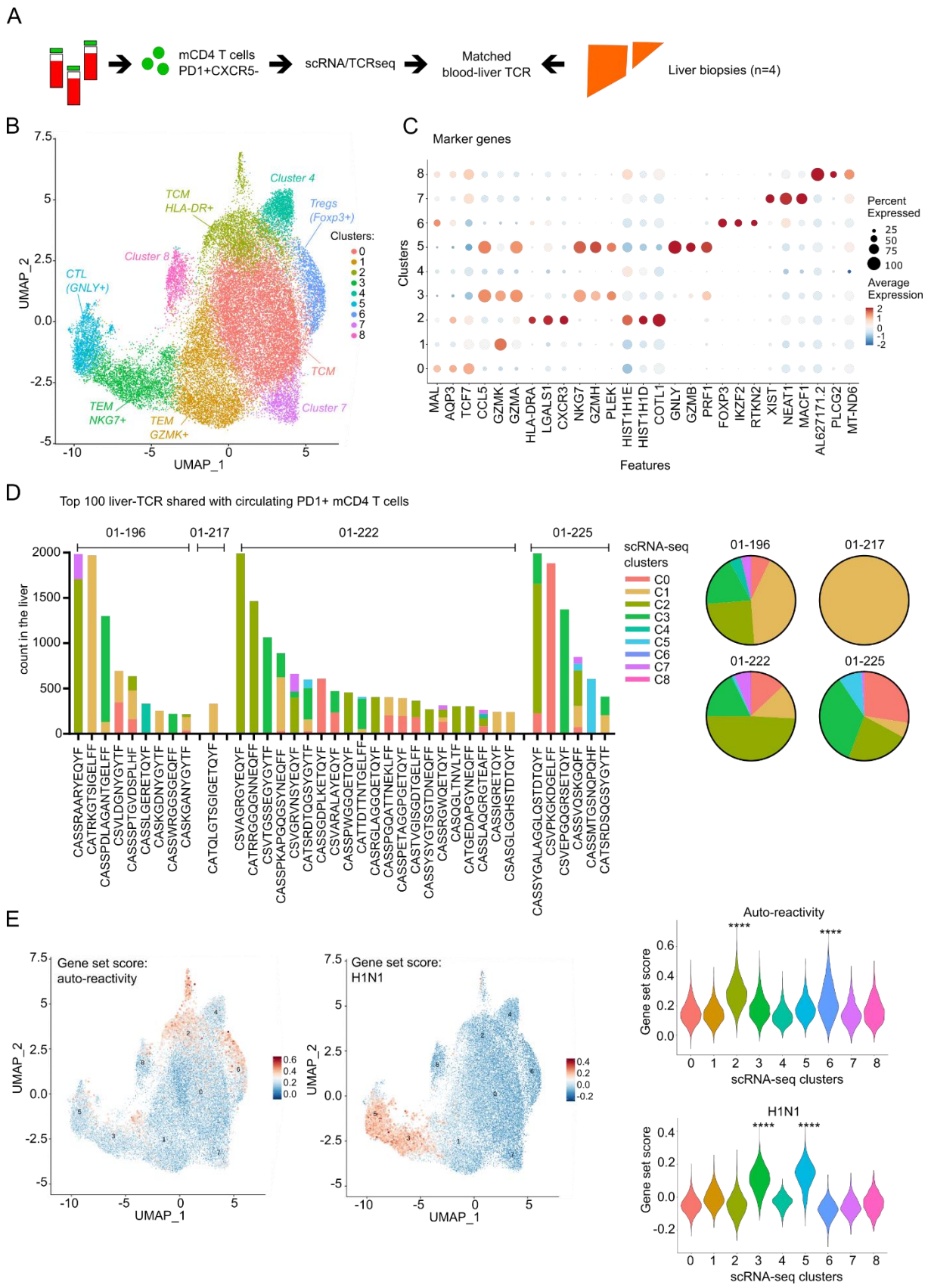

578

579 **Figure 3. Tracking TCR clonotypes between liver biopsies and circulating CD4 T cell subsets.** (A) Experimental design for
580 scRNA-seq and TCR-seq of memory PD1+ CXCR5- CD4 T cells from four distinct AILD patients. (B) UMAP representation of
581 circulating memory PD1+ CXCR5- CD4 T cell transcriptomes, colored by non-supervised Louvain clustering. (C) Dot plot
582 representation of top 3 marker genes of each clusters in (B). (D) Frequency representation ('counts') of each top 100 largest

583 liver TCRβ sequences found in circulating PD1+ mCD4 T cells. For each TCRβ sequences the cluster affiliation is indicated
584 based on scRNA-seq and TCR-seq of memory PD1+ CXCR5- CD4 T cells. Pie chart represent the global cluster affiliation of the
585 top 100 largest liver TCRβ sequences found in circulating PD1+ mCD4 T cells per patient. (E) Left: UMAP representation of
586 circulating memory PD1+ CXCR5- CD4 T cell transcriptomes colored by gene set score for the indicated antigen-reactivity
587 module. Right: violin plots of gene set score distribution of cells from different Louvain clusters, as indicated. Pairwise
588 comparison with Benjamini-Hochberg corrected Wilcoxon test. ****: p<0.0001.

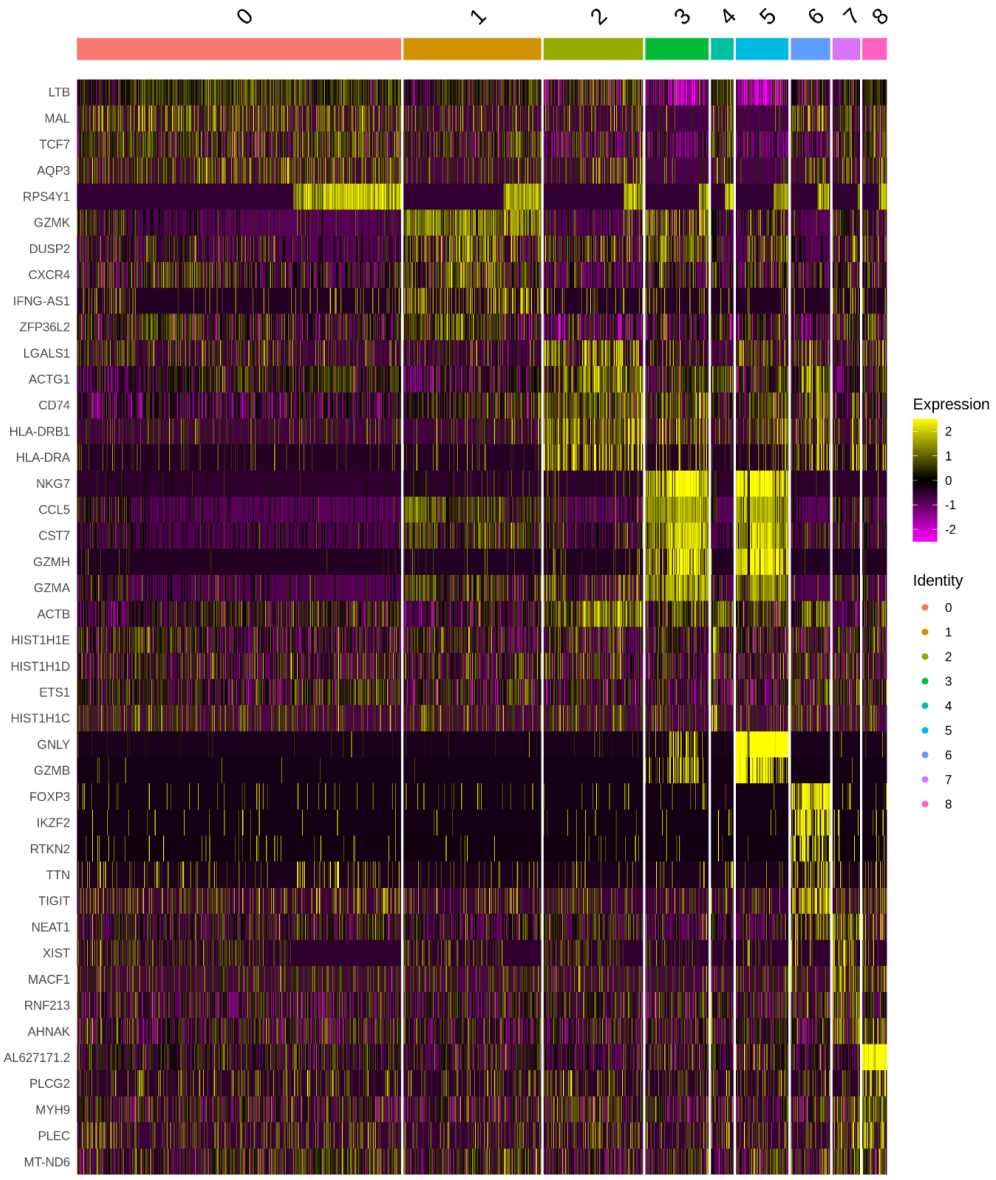

589

590 **Supplementary figure 5: Single cell gene expression heatmap for top 5 marker genes of PD1+ CXCR5- memory CD4 T cells.**

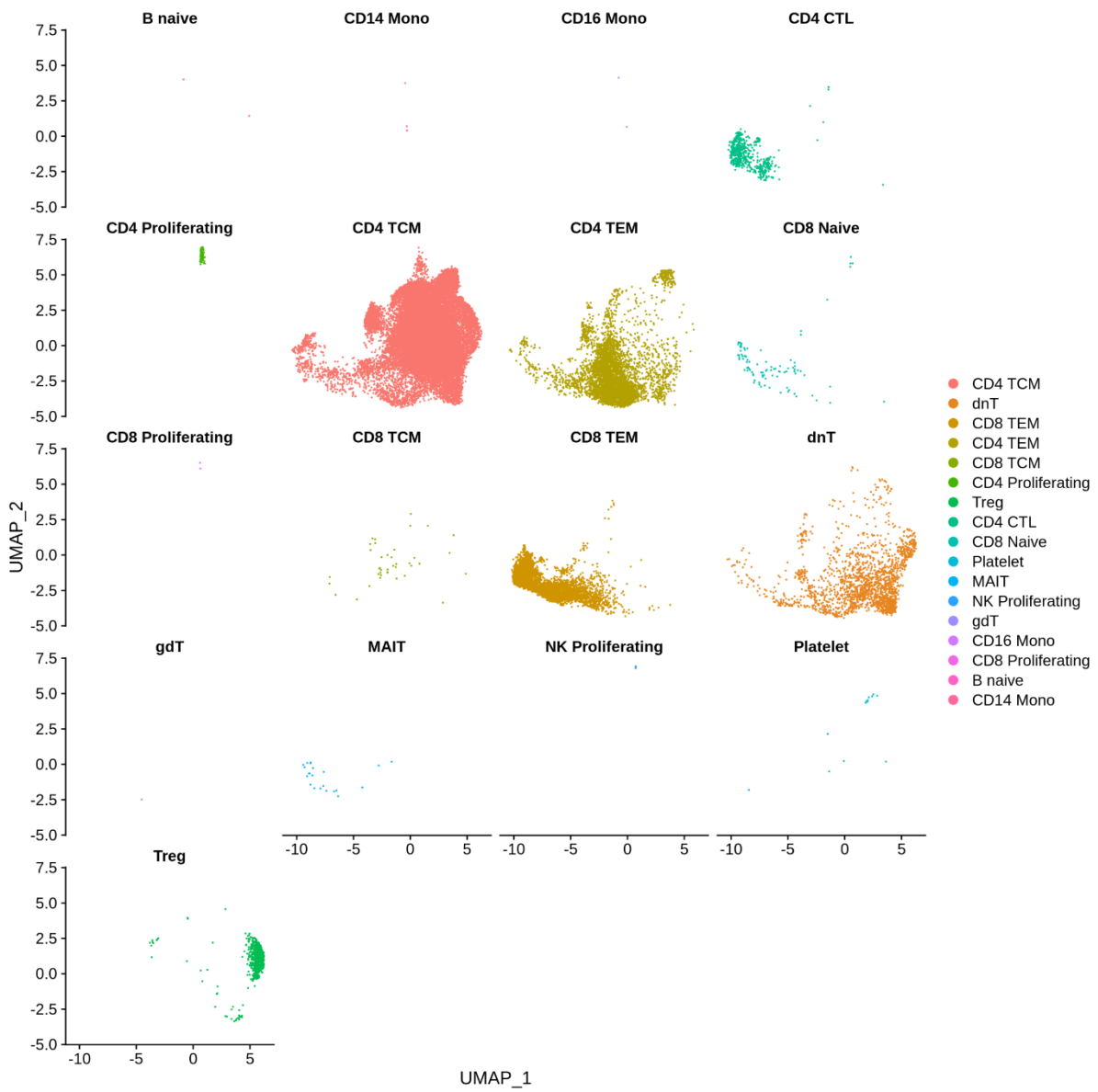

Supplementary figure 6: Unsupervised azimuth annotation of PD1+ CXCR5- memory CD4 T cell subsets.

We further sought to relate the transcriptional signatures of peptide-stimulated and untouched circulating autoreactive mCD4 T cells (Figure 2 and 3). Based on previously published results (Renand et al), we synthesized HLA-DRB1 03:01 biotinylated monomers loaded with the Sepsecs$_{187\text{-}197}$ epitope peptide, assembled fluorescent-labeled pMHCII tetramers, and monitored Sepsecs-specific CD4 T cells in the blood of six SLA+ HLA-DR3+ patients (Figure 4A). Peptide-MHCII tetramer positive (TTpos) CD4 T cells were detectable and displayed a PD1+ memory phenotype (Figure 4B). We performed plate-based single-cell transcriptomic analyses of pMHCII TTpos Sepsecs-specific CD4 T cells. We compared pMHCII TTpos and TTneg CD4 T cells for their expression of gene modules associated with antigen reactivities defined in Figure 2 (Figure 4C) and in the PD1+ CXCR5- mCD4 T cell subsets identified in Figure 3 (Figure 4D). As expected, pMHCII TTpos CD4 T cells expressed significantly higher levels of gene modules associated to self-antigen specific CD4 T cells (Figure 4C) and cluster 2 TCM HLA-DR+ CD4 T cells (Figure 4D).

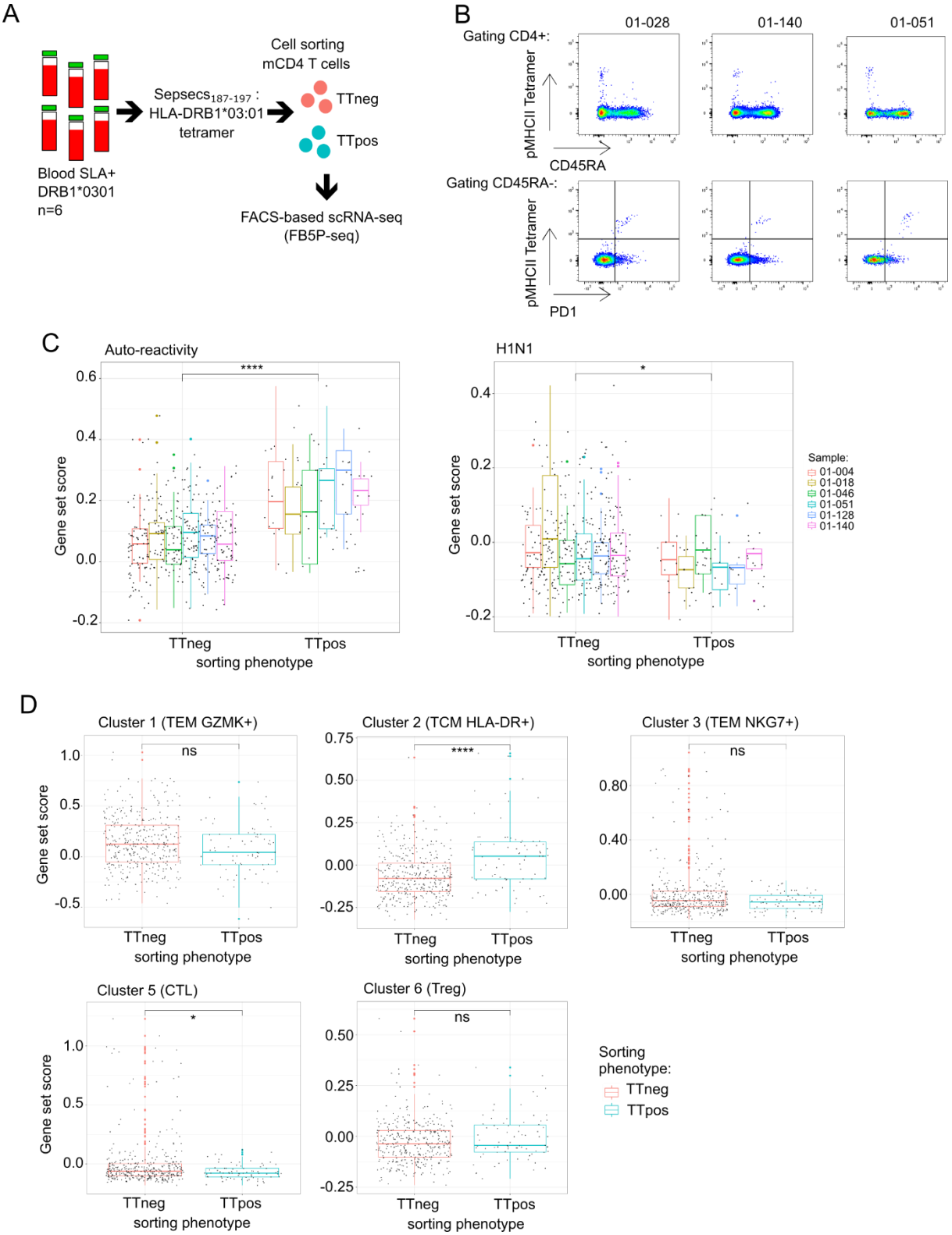

Figure 4. Single cell transcriptomic analysis of unstimulated Sepsecs-specific CD4 T cells. (A) Experimental design for scRNA-seq data analysis of Sepsecs/SLA$_{185-197}$ HLA-DRB1*0301 pMHCII tetramer positive cells. (B) Pseudocolor dot plot representation of pMHCII tetramer staining in three of six patients. Top: surface expression of CD45RA and pMHCII tetramer in CD4+ T cells. Bottom: surface expression of PD1 and pMHCII tetramer in CD4+ CD45RA- T cells. (C) Box plots of gene set score distribution of pMHCII tetramer negative (TTneg) or positive (TTpos) cells for antigen reactivity modules as indicated. (D) Box plots of gene set score distribution of pMHCII tetramer negative (TTneg) or positive (TTpos) cells for top marker genes of circulating memory PD1+ CXCR5- CD4 T cell clusters defined in Figure 3E. Unpaired Mann-Whitney test was used: *: p<0.05; ****: p<0.0001.

614 Altogether, our integrative analyses of circulating self-antigen-specific and dominant intrahepatic CD4
615 T cell clones in AILD patients converge to establish that some autoreactive CD4 T cell clones can be
616 found both in the liver and in the blood, where they are defined as PD1+ CXCR5- HLA-DR+ mCD4 T
617 cells, with a specific B-helper and immuno-exhausted transcriptional profile.

618 - **High-dimensional phenotyping of circulating liver-autoreactive CD4 T cells.**

619 We then examined the precise phenotype of these circulating liver-autoreactive CD4 T cells by spectral
620 flow cytometry on PBMC from patients affected by different liver diseases: five control non-
621 autoimmune patients with non-alcoholic steatohepatitis (NASH), fourteen AIH patients with an active
622 disease, and thirteen AIH patients in remission under treatment (Supplementary Table 2). We focused
623 on the mCD4 T cell population and performed clustering analysis (Figure 5A-D). The comparison
624 revealed the significant increase of three cell clusters in patients with active AIH in comparison to NASH
625 patients (C6, C12 and C15, Figure 5B). Both C6 and C15 clusters were TCM CD27+ TIGIT+ PD1+ CXCR5-
626 CD49d+ CD25- CD127- ICOS+ CD4 cells and expressed CD38, a marker we have already observed
627 upregulated by CD4 T cells during active AIH[22] (Figure 5C and D, Supplementary Figure 7).The C15
628 cluster was characterized by high HLA-DR expression and may represent the liver-autoreactive CD4 T
629 cells identified previously (Figure 3). This cluster (C15) was high in the blood of active AIH patients
630 compared to AIH patients in remission under treatment (Supplementary Figure 7). The C12 cluster was
631 characterized by CD57 expression but its frequency was very low. We performed a supervised analysis
632 of the HLA-DR+ subset and confirmed that it was significantly more frequent during the active phase
633 (AIHa) than in patients with NASH or in remission (AIHr) (Supplementary Figure 8). In parallel, in four
634 active AIH patients, we performed the intracellular analysis of the PD1+ TIGIT+ CXCR5- CD4 subset with
635 a new panel of antibodies. We confirmed its heterogeneity; this subset consisted of classical Treg
636 (FOXP3+ CD127- EOMES-), cytotoxic cells (GZMB+ HLA-DR- EOMES+ GZMA+) and HLA-DR+ FOXP3-
637 EOMES- cells (Supplementary Figure 9). This was in agreement with the transcriptomic data (Figure 3)
638 to demonstrate that the liver-autoreactive CD4 T cell cluster (HLA-DR+ PD1+) was different from the
639 Treg and cytotoxic (CTL) CD4 T cell clusters. Thus, after exclusion of Tregs (using CD127 and CD25 or
640 FOXP3 expression), HLA-DR expression emerged as the most relevant marker for delineating liver-
641 autoreactive CD4 T cells among PD1+ TIGIT+ CD4 T cells.

642 To get an insight into the functionality of these rare cells, we used this strategy of Treg exclusion to
643 sort HLA-DR+ PD1+ TIGIT+ CXCR5- mCD4 T cells and to perform their TCR stimulation *in vitro* for bulk-
644 RNA sequencing (Figure 5E and F). Like autoreactive CD4 T cells after peptide stimulation, HLA-DR+
645 PD1+ TIGIT+ CXCR5- mCD4 T cells significantly upregulated *CXCL13*, *IL21*, *CTLA4*, *PRDM1*, *TIGIT*, *MAF*
646 and *TOX,* upon TCR stimulation. These cells also expressed *LGALS1*, *CXCR3, HLA-DR and CD74* like CD4
647 TCM HL-DR+ cells*;* these genes were downregulated by TCR stimulation. They expressed genes linked
648 to the TPH and TRM CD4 cell signature like *CD39, TIM3, CXCR6, CCR5* and *CCR2* that link this cell to the
649 tissue immune response. They could also express *TNF* and *INFG*, but not *IL2*, after TCR stimulation. This
650 subset presented high proximity with autoreactive CD4 T cells and circulating dominant intrahepatic
651 clonotype, thus, we can conclude that HLA-DR+ PD1+ TIGIT+ CXCR5- CD4 T cells contained the liver-
652 autoreactive CD4 T cells.

653 We performed a spatial multi-phenotyping analysis on a liver biopsy from one AIH patient, and we
654 identified tertiary lymphoid structures characterized by the presence of B-cells (CD20+ cells) and
655 follicular dendritic cells (FDC, CD21+) (Figure 5G, and Supplementary Figure 10). Interestingly, PD1+
656 CD4 T cells were enriched in the FDC and B cell zones, in comparison to the CD8+ and the PD1- CD4 T
657 cells (Figure 5H and I, supplementary Figure 10). The FDC area was enriched in CXCR5+ cells suggesting
658 germinal center formation and/or B cell retention (Figure 5I). Although the phenotype of the PD1+

659 CD4+ T cells was less detailed, this localization suggested that liver-autoreactive CD4 T cells could be
660 involved in the B-cell response within the liver.

Group	Active AIH (AIHa)	Remission AIH (AIHr)	NASH
	n=14	n=13	n=5
Age (year)	50,3 [39,7-61]	52,5 [39,1-65,8]	59,2 [33,3-85,1]
Female, n (%)	9 (64%)	9 (69%)	3 (60%)
IgG (g/L)	19,5 [15,2-23,8]	11,4 [9,9-12,9]	11,9 [6,8-17,1]
AST (IU/L)	307 [121,7-492,1]	22,6 [17,4-27,9]	45,9 [23,4-68,4]
ALT (IU/L)	505 [185,6-824,7]	20,8 [14,4-27,1]	73,5 [6,2-140,9]
Immunosuppressive agents n (%)			
No, n (%)	9 (64%)	0	5 (100%)
Naïve	9	0	NA
Yes, n (%)	5 (36%)	13 (100%)	0
Azathioprin	4	11	NA
MMF	1	1	NA
Steroids only	0	1	NA
Steroids associated to other therapy	2	3	NA

661 *AIH: Autoimmune Hepatitis, NASH: Non Alcoholic Steatohepatitis, AST: Aspartate Aminotransferase, ALT: Alanine*
662 *Aminotransferase, NA: non-applicable*

663 **Supplementary Table 2**. Clinical and biological characteristics of patients with AIH and NASH expressed as mean [95%
664 confidence interval].

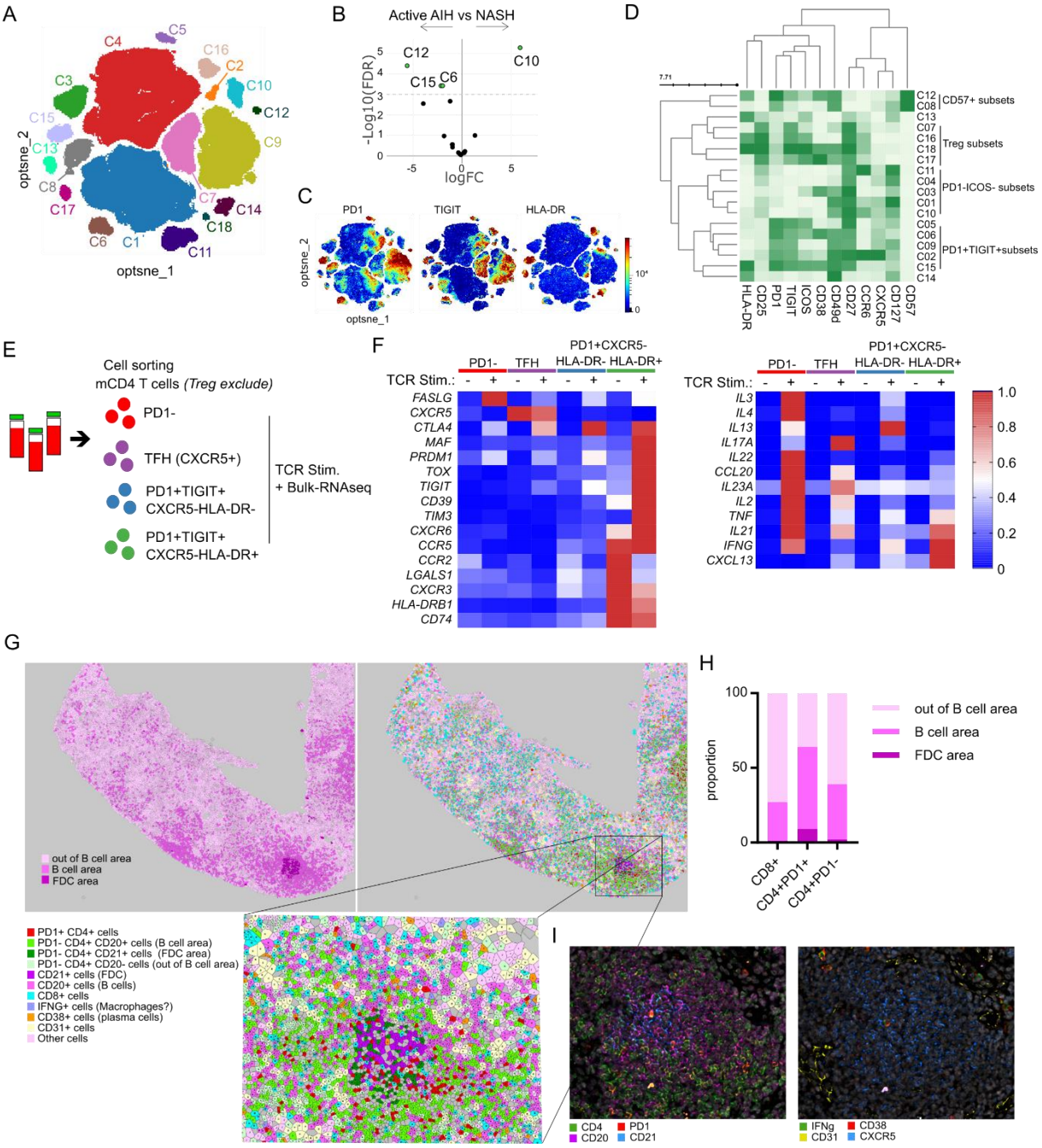

Figure 5: Characterization of circulating PD1+ TGIT+ HLA-DR+ non-Treg CD4 T cells as liver-autoreactive CD4 T cells. (A) Tsne representation of blood memory CD4 T cell subsets, colored by non-supervised FlowSOM clustering, from 5 control non-autoimmune patients with non-alcoholic steatohepatitis (NASH), 14 AIH patients with an active disease (Active AIH), and 13 AIH patients in remission under treatment. (B) Differential cluster abundance between active AIH and NASH patients. (C) PD1, TIGIT and HLA-DR expression. (D) Surface marker heatmap of the clusters identified in (A). (E) Experimental design for bulk-RNA-seq after cell sorting and 24h *in vitro* TCR stimulation. (F) Selected genes heatmap of indicated CD4 T cell subsets after or not TCR stimulation from five distinct patients (mean representation). (G) Voronoi representation of cellular subsets in an AIH liver biopsy after cell segmentation. FDC area is defined by expression of CD21; B cell area is defined by CD20 expression; and out of B cell area is defined by the absence of CD20 expression. The lower panel shows a zoom on the selection indicated in the upper panel. (H) Representation of the repartition of CD8+, CD4+ PD1+ and CD4+ PD1- cells in FDC, B cell and out of B cell area defined in (G). (I) CD4, CD20, PD1, CD21, IFNg, CD38, CD31 and CXCR5 marker staining within segmentation.

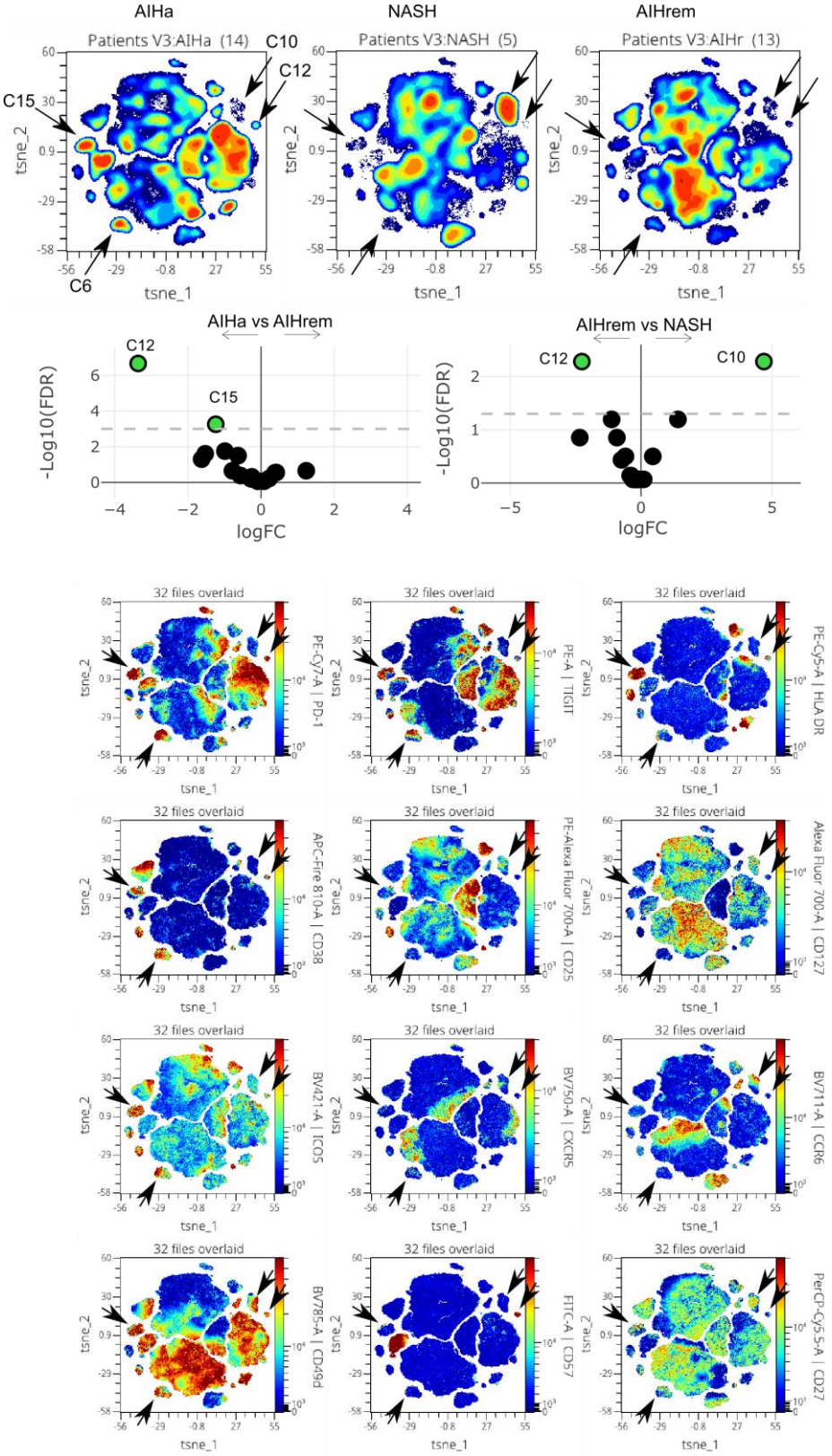

Supplementary figure 7: Detailed unsupervised flow cytometry analysis of active AIH (AIHa), NASH and AIH in remission (AIHrem) patients and expression of indicated markers on the Tsne representation of blood memory CD4 T cell subsets.

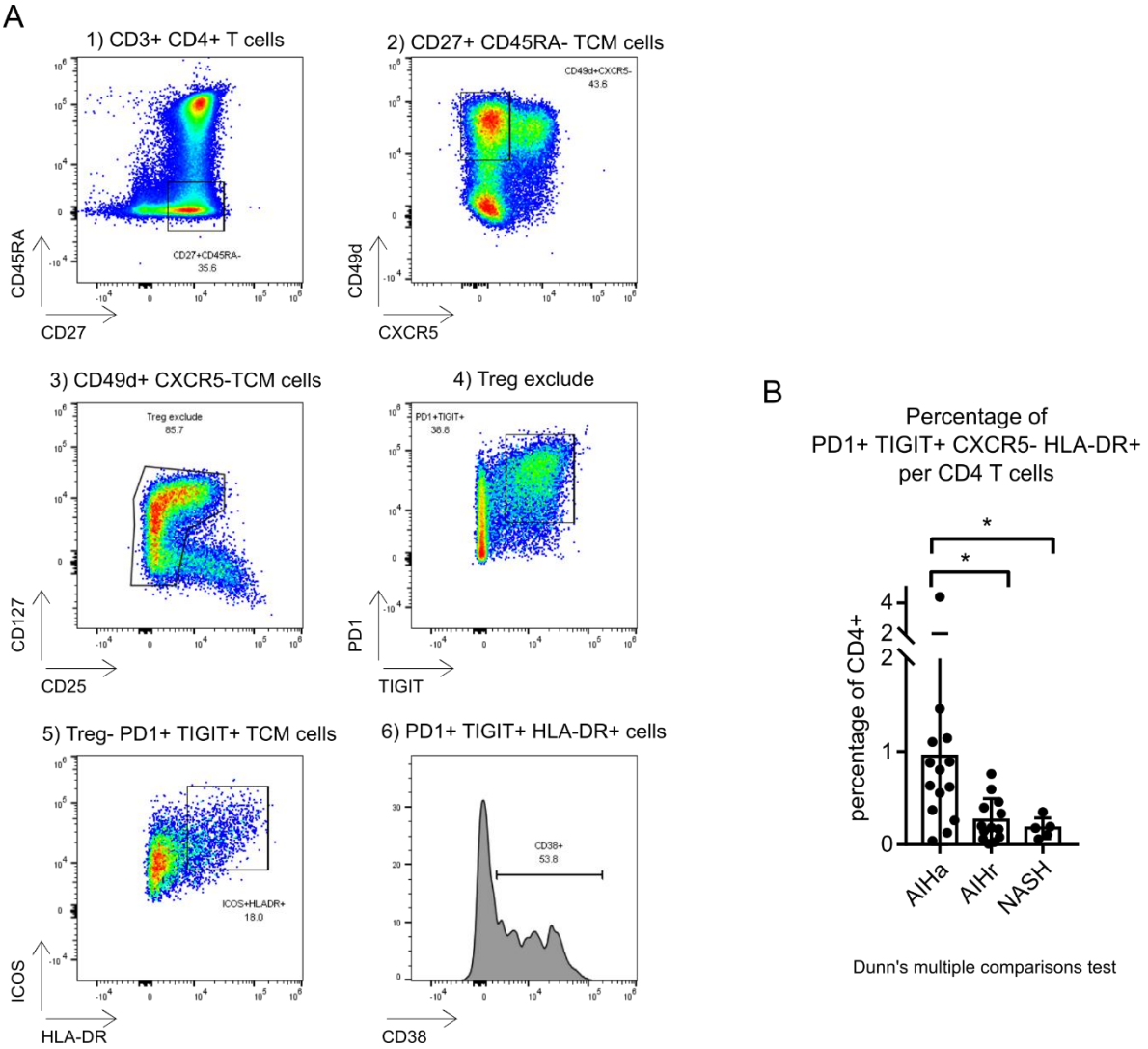

Supplementary figure 8: Supervised identification of the cluster 08 (PD1+ CXCR5- TIGIT+ HLA-DR+). (A) dot plot representation of the gating strategy. (B) Frequency of PD1+ CXCR5- TIGIT+ HLA-DR+ CD4 T cells per total CD4+ T cells in the blood of 5 NASH, 14 active AIH (AIHa), and 13 AIH patients in remission (AIHr) under treatment (<2 years, n=4; >2years, n=12).

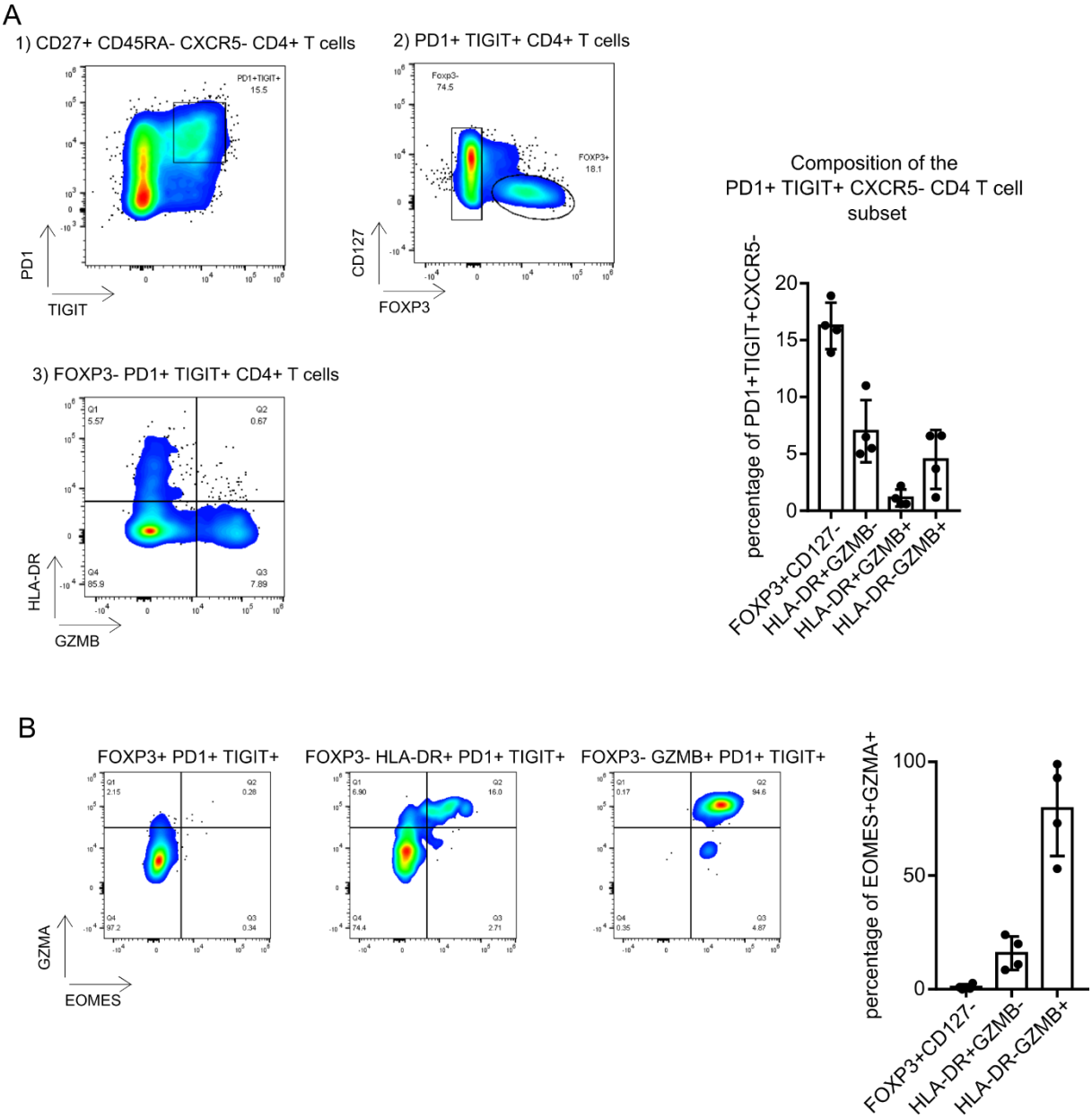

Supplementary figure 9: Intracellular characteristics of PD1+ CXCR5- TIGIT+ memory CD4 T cells. (A) Foxp3, Granzyme B (GZMB) and HLA-DR expression within PD1+ CXCR5- TIGIT+ memory CD4 T cells. (B) Eomes and GZMA expression by PD1+ CXCR5- TIGIT+ FOXP3+ (FOXP3+ CD127-); PD1+ CXCR5- TIGIT+ FOXP3- HLA-DR+ (HLA-DR+ GZMB-) and PD1+ CXCR5- TIGIT+ GZMB+ memory CD4 T cells (HLA-DR- GZMB+).

A

DAPI+ → CD31+ (Epithelial cells)
↓
CD31- → IFNG+ (Macrophages?)
↓
IFNG- → CD38+ (Plasmocytes)
↓
CD38- → CD21+ (FDC area) → CD4+ → PD1+ (PD1+ CD4+ T cells in FDC area)
PD1- (PD1- CD4+ T cells in FDC area)
↓
CD4- → CD8+ (CD8+ T cells in FDC area)
↓
CD8- (FDC)

CD21- → CD20+ (B cell area) → CD4+ → PD1+ (PD1+ CD4+ T cells in B cell area)
PD1- (PD1- CD4+ T cells in B cell area)
↓
CD4- → CD8+ (CD8+ T cells in B cell area)
↓
CD8- (B cells)

CD20- (out of B cell area) → CD4+ → PD1+ (PD1+ CD4+ T cells out of B cell area)
PD1- (PD1- CD4+ T cells out of B cell area)
↓
CD4- → CD8+ (CD8+ T cells out of B cell area)
↓
CD8- (Other cells)

B

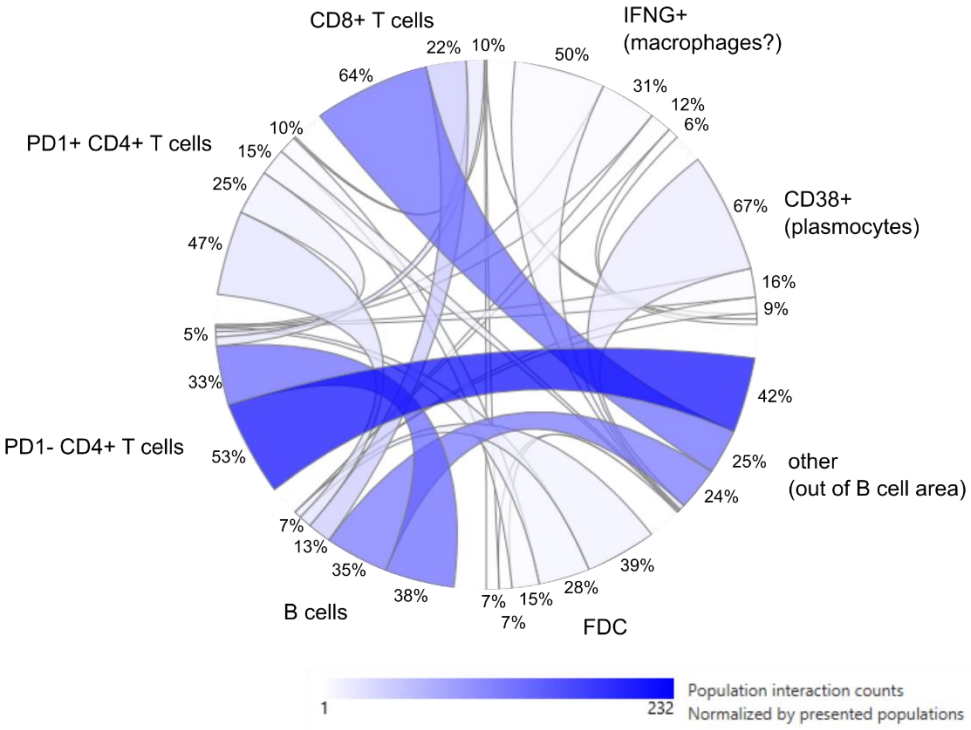

Supplementary figure 10: Spatial lineage assignment strategy and proximity analysis. (A) Schematic lineage assignment strategy. (B) Proximity analysis between major cellular subsets identified. Analysis performs with the Multiple Analysis Viewer (MAV) software.

694 • **The transcriptomic signature of liver-autoreactive CD4 T cells is dictated by the hepatic**
695 **environment**

696 Since circulating liver-autoreactive CD4 T cells have a specific transcriptomic signature in humans, we
697 investigated whether their molecular profile was due to antigen reactivity in the hepatic environment
698 or to a lineage-specific signature. To answer this question, we designed a non-TCR-transgenic mouse
699 model that allows the analysis of the emergence and modulation of CD4 T cell responses against a
700 model antigen expressed by hepatocytes. We used a model of Balb/c mice in which the hemagglutinin
701 (HA) expression was restricted to hepatocytes, by an inducible Cre recombinase under the control of
702 hepatocyte-specific mTTR (transthyretin) promotor (HA/iCre) (Figure 6A and Supplementary Figure
703 11). Tamoxifen alone was used to induce HA expression in the liver of HA/iCre mice (Figures 6A and B).
704 Tamoxifen-induced HA expression in the liver alone did not induce an anti-HA humoral response
705 (Figure 6C). Intramuscular injection of a Cre-coding adenovirus (AdCre) or a HA-coding plasmid was
706 performed to generate peripheral immunization against the HA antigen (HA i.m, Figure 6A). Anti-HA
707 antibodies were measured only after peripheral HA-specific immunization (Figure 6C). HA-specific
708 memory ($CD44^{high}$) CD4 T cells were detected with pMHCII tetramer in the spleen of mice after
709 peripheral immunization. Regarding the immune response in the liver, we neither detected HA-specific
710 CD4 T cells after peripheral immunization nor in tamoxifen-treated mice (Figure 6D).

711 To analyze HA-specific CD4 T cells in the liver, we induced HA expression in the liver, by using tamoxifen
712 in pre-immunized HA/iCre mice (HA i.m + Tamoxifen, Figure 6A); we used littermates lacking liver-
713 restricted expression of an inducible Cre recombinase (Ctrl) as control (Supplementary Figure 11). In
714 this condition, we detected HA-specific CD4 T cells only in the liver of immunized mice expressing HA
715 by hepatocytes after tamoxifen treatment (Figure 6D), showing active recruitment from the periphery
716 of HA-specific memory CD4 T cells into the liver following local antigen expression. In addition, liver
717 HA-specific CD4 T cells expressed high levels of PD-1 (Figure 6E).

718 In this mouse model, we analyzed the transcriptomic profile of HA-specific CD4 T cells in mouse liver
719 and spleen. Overall, all spleen HA-specific CD4 T cells, irrespective of liver HA expression, clustered
720 together, whereas liver HA-specific CD4 T cells show a distinct transcriptomic signature (Figure 6F and
721 G). Besides expressing genes associated with the inflammatory response (e.g. *Ox40*, *CD137*, *Ccl5* and
722 *Icos*), liver HA-specific CD4 T cells expressed genes involved in the regulation of proliferation and
723 activation (e.g. *Tigit*, *Ctla4*, *Prdm1* and *Casp3*) (Figures 6H). Comparative analysis with liver-self-antigen
724 specific transcriptomic signature revealed four common pathways linked to the regulation of T cell
725 activation (GO:0042110 T cell activation; GO:0002694 reg. of leukocyte activation; GO:0051249 reg. of
726 lymphocyte activation; GO:0050863 reg. of T cell activation). The analysis of the genes from these
727 pathways revealed common genes shared between liver HA-specific CD4 T cells in mice and circulating
728 liver-autoreactive CD4 T cells in human (Figure 6I). Both cell types expressed high levels of TIGIT, CTLA-
729 4, BATF and PRDM1 gene expression. These data demonstrate immuno-regulatory genes were induced
730 during local immune response in the liver. These suggest that the immune signature of human
731 circulating liver-autoreactive CD4 T cells is an imprint of the hepatic environment, and could suggest
732 that these cells leak out of damaged tissue after a phase of high reactivity in the tissue.

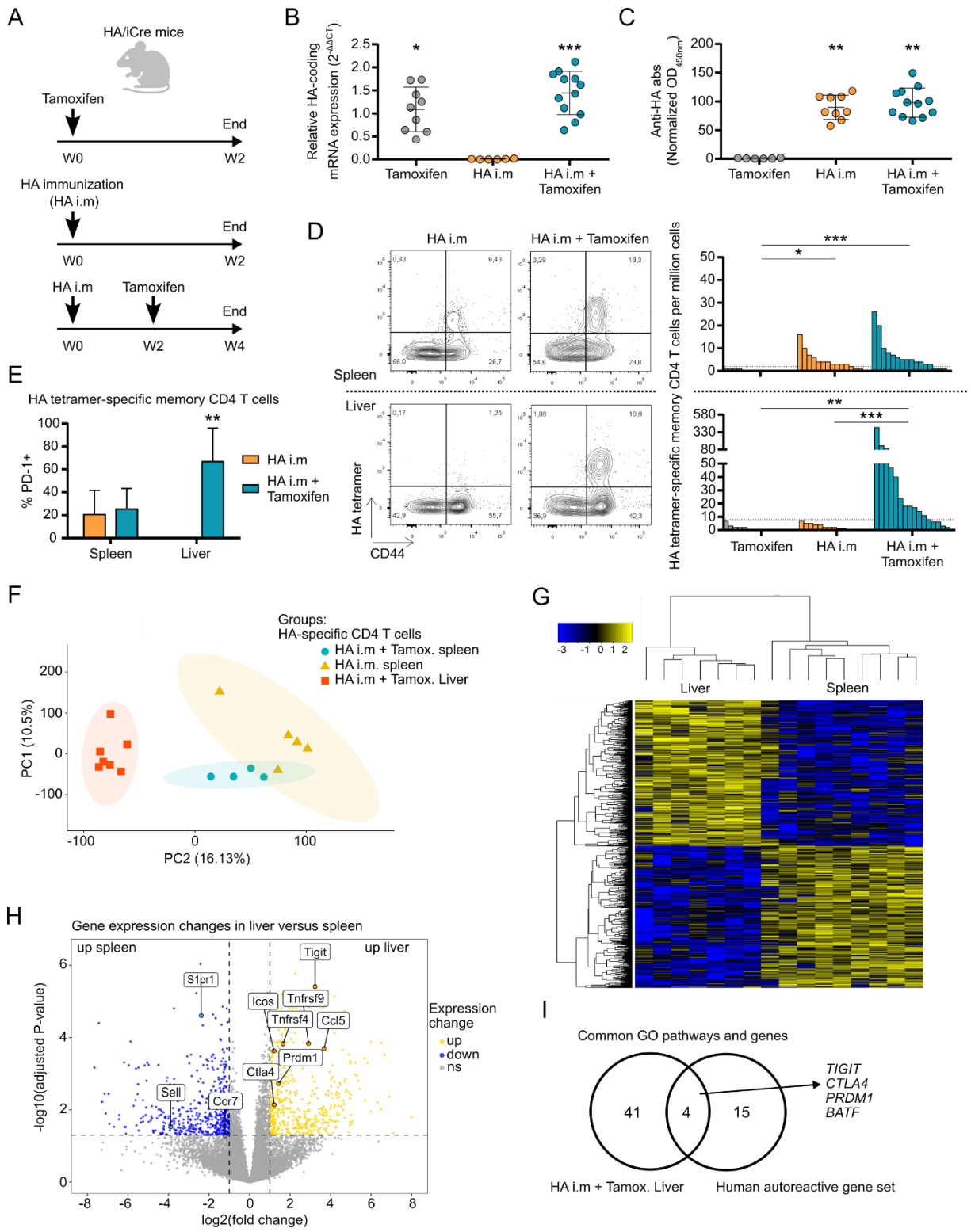

Figure 6: Analysis of antigen-specific CD4 T cells from the liver and the spleen of an in vivo non-TCR-transgenic mouse model. (A) Experimental design for investigation of immune response against the HA antigen in the liver. HA/iCre mice received either tamoxifen treatment (n=9), HA immunization treatment (HA i.m; n=15), or HA immunization followed 2 weeks later by tamoxifen treatment (HA i.m + Tamoxifen; n=12). Mice were euthanized 2 weeks after the last treatment. (B) Relative HA mRNA expression in the liver. β-actine was used as loading control. (C) Analysis of normalized anti-HA antibody rate in serum of mice. (D) Analysis of HA-tetramer-specific CD4 T cells in the spleen (top) and in the liver (bottom). Contour plot representation of HA tetramer staining and CD44 expression in CD4 T cells from HA i.m and HA i.m + Tamoxifen mice (left). Frequency of HA-tetramer-specific memory ($CD44^{high}$) CD4 T cells per million cells (right). Dotted lines in the frequency graphs represent threshold of positive detection of HA-specific CD4 T cell population. (E) Analysis of PD-1 expression in detectable

743 HA-specific memory CD4 T cells from the spleen and the liver of HA i.m and HA i.m + Tamoxifen mice. (F) Principal component
744 analysis (PCA) of bulk-RNA-seq transcriptome of HA-specific CD4 T cells isolated from the liver or the spleen. (G) Gene
745 expression heatmap of HA-specific CD4 T cells. (H) Volcano plot of gene expression change between liver and spleen HA-
746 specific CD4 T cells. (I) Genes from GO enrichment pathways upregulated and shared between mouse liver HA-specific CD4 T
747 cells and human autoreactive CD4 T cells. Dunn's multiple comparisons test was used for B, C and D. Mann-Whitney test was
748 used for E. *: $p<0.05$; **: $p<0.01$; ***: $p<0.001$.

749 • **Induction of immune checkpoint molecules on CD4 T cells by the hepatic environment**
750 **contribute to local tolerance**

751 The upregulation of immune checkpoint molecules by the antigen-specific CD4 T cells after their
752 reactivity in the liver suggested the potential regulation of these cells by the hepatic environment.
753 Therefore, we blocked PD-1 and CTLA-4 pathways, using immune checkpoint inhibitors (ICI) antibodies,
754 in our mouse model of hepatic infiltration by HA-specific CD4 T cells, after immunization and induction
755 of HA expression by hepatocytes (Figure 7A). Data reveal a significant hepatitis marked by high
756 histological liver inflammation score, only when mice receiving ICI are pre-immunized and express HA
757 in the liver (HA/iCre + ICI, Figures 7B and C). Mice immunized but unable to express HA in their liver
758 after tamoxifen treatment did not show significant liver inflammation after PD-1 and CTLA-4 blockade
759 (Ctrl + ICI, Figures 7B and C). These data suggest that the hepatic environment specifically regulates
760 the antigen-specific response by engaging immune checkpoint receptors.

761 Then, we assessed the role of CD4 T cells in this response by depleting CD4+ cells with anti-CD4
762 antibodies in immunized HA/iCre mice treated with tamoxifen and PD-1/CTLA-4 blocking antibodies
763 (Figure 7D). First, CD4 depletion was associated with significantly lower immunization rate according
764 to anti-HA antibody seric level (Figure 7E). Interestingly, histological analysis revealed significantly
765 reduced liver damages in CD4 depleted mice, showing major role of CD4 T cells in promoting liver
766 inflammation in our model (Figures 7F and G). The hepatic inflammation observed after PD-1 and CTLA-
767 4 blockade was linked to substantial HA-specific CD8 response in the spleen and in the liver, but
768 depletion of CD4 T cells before the induction of HA expression in the liver abrogated the HA-specific
769 CD8 response (Figure 7H). These results demonstrate that the hepatic environment quickly regulates
770 local immune response against an antigen expressed by hepatocytes through upregulation of immune
771 checkpoint pathways in a CD4-dependent manner.

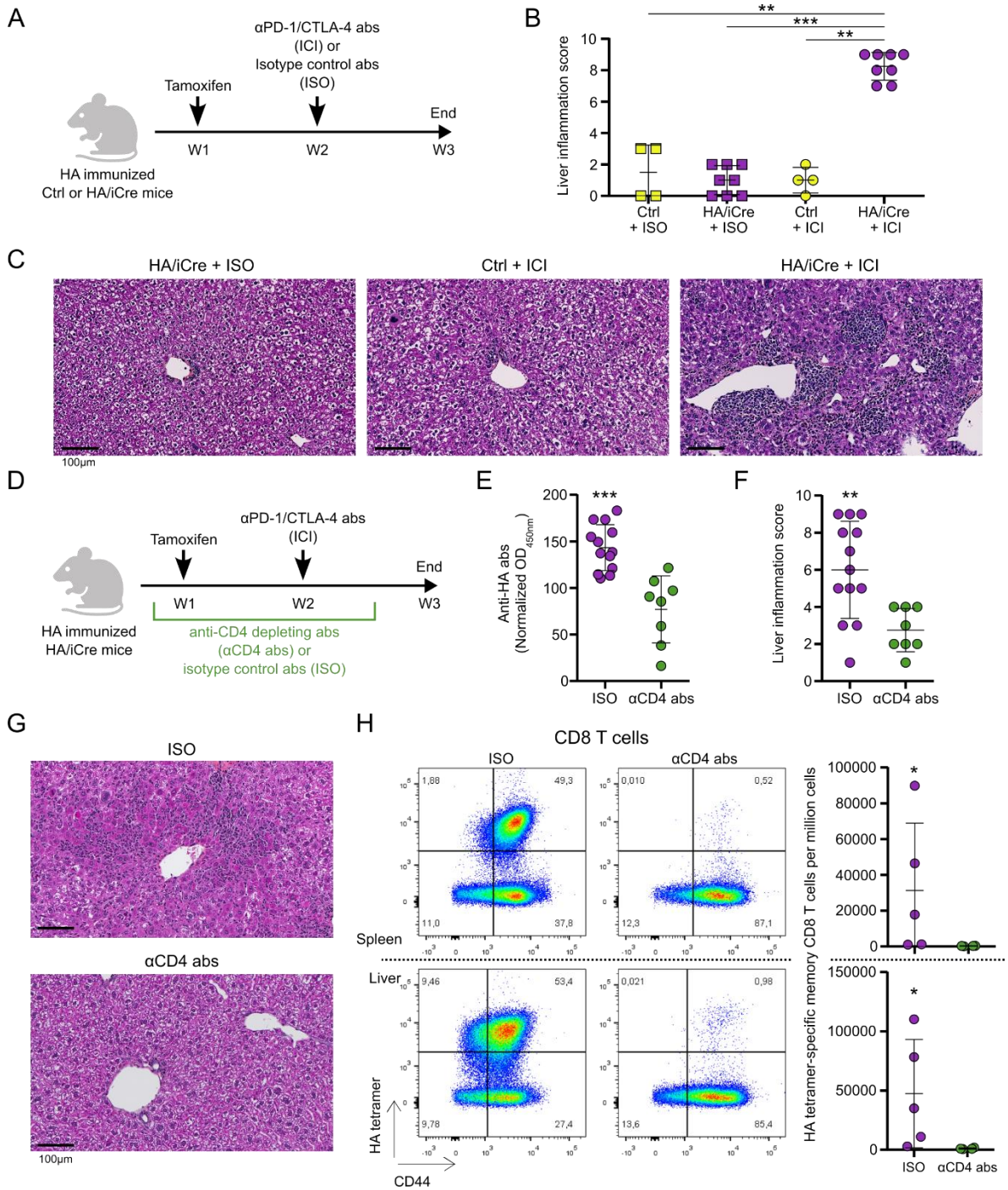

Figure 7: Immune checkpoint pathways control liver antigen-specific CD4 T cell responses and mediate hepatic tolerance. (A) Experimental design for PD-1 and CTLA-4 blockade (ICI) in HA immunized tamoxifen-treated HA/iCre mice. Injection of isotype control antibodies to ICI was used as control (ISO). (B) Histological liver inflammation scoring analysis of liver tissue sections from immunized tamoxifen-treated control (Ctrl; n=8) and HA/iCre (n=16) mice treated either with isotype control antibodies (+ ISO; Ctrl: n=4, HA/iCre: n=8) or anti-PD-1 and anti-CTLA-4 blocking antibodies (+ ICI; Ctrl: n=4, HA/iCre: n=8). (C) Representative pictures of paraffin-embedded liver sections stained with HPS coloration from indicated conditions. Black line is used as scale. (D) Experimental design for CD4 depletion (αCD4 abs) in immunized tamoxifen-treated HA/iCre mice receiving PD-1 and CTLA-4 blockade protocol (n=13). Injection of isotype control antibody to αCD4 abs was used as control (ISO; n=8). (E) Analysis of normalized anti-HA antibody rate in serum of mice. (F) Histological liver inflammation scoring analysis of liver tissue sections. (G) Representative pictures of paraffin-embedded liver sections stained with HPS coloration from indicated conditions. Black line is used as scale. (H) Pseudocolor dot plot representation of HA tetramer staining and CD44 expression in CD8 T cells from spleen (top) and liver (bottom) of ISO (n=5) and αCD4 abs (n=4) mice (left). Frequency of HA tetramer-specific memory ($CD44^{high}$) CD8 T cells per million cells (right). Mann-Whitney test was used for B, E, F and H. *: $p<0.05$; **: $p<0.01$; ***: $p<0.001$.

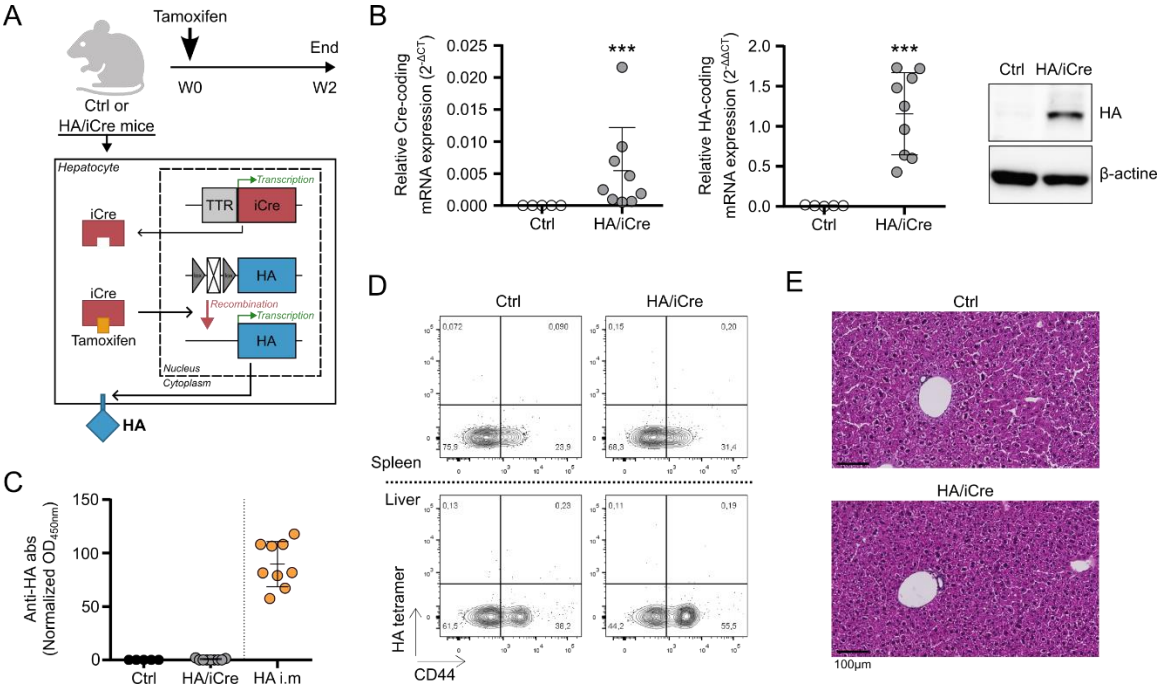

Supplementary Figure 11: Tamoxifen treatment in non-TCR-transgenic mouse model. (A) Experimental design and schematic illustration for tamoxifen treatment in Rosa26 HA floxed mice (Ctrl) and Rosa26 HA floxed TTR-inducible Cre mice (HA/iCre). (B) Relative Cre mRNA expression (left) and relative HA mRNA expression (middle) in the liver. HA protein detection from total protein extract of liver samples (left). β-actine was used as loading control. (C) Analysis of normalized anti-HA antibody rate in serum of tamoxifen-treated Ctrl and HA/iCre mice. Anti-HA antibody rate of immunized mice (HA i.m) was indicated as positive control. (D) Contour plot representation of HA tetramer staining and CD44 expression in CD4 T cells from spleen (top) and liver (bottom) of tamoxifen-treated Ctrl and HA/iCre mice. (E) Representative pictures of paraffin-embedded liver sections stained with HPS coloration. Black line is used as scale. Mann-Whitney test was used for B. ***: p<0.001.

Discussion

In this study, we analyzed the transcriptomics, TCR profile and single-cell protein expression of circulating liver-self-antigen-specific CD4 T cells and expanded intrahepatic CD4 T cell clonotypes found in the blood of AILD patients. We have identified in the bloodstream a subset of liver-autoreactive CD4 T cells with an autoimmune transcriptomic profile (*CXCL13, IL21, TIGIT, PRDM1*, *TOX, HLA-DR…*) that is linked to a clonal expansion in the liver. Our results, using a mouse model to track the early immune response against an antigen expressed in the liver, revealed that liver antigen-specific CD4 T cells acquired an immuno-exhausted (*TIGIT, PRDM1, CTLA4)* transcriptomic signature comparable to that of circulating liver-autoreactive CD4 T cells in AILD patients. Our data support the idea that circulating liver-autoreactive CD4 T cells are liver-derived autoreactive CD4 T cells and that their transcriptomic signature is imprinted by antigen reactivity in the tissue. The ability to identify a subset of T cells linked to tissue autoreactivity in blood opens important prospects for the development of biomarkers and therapies. These cells can be identified and isolated from blood for further characterization using *in vitro* assays to develop new therapies. Our study is in line with the recent publication by Yossef et al, who report that the signature of tumor-specific CD8 T cells in blood shares similarities with their counterparts in tissues and could therefore be an alternative source for identifying antitumor T cell reactivity[41].

We also report for the first time a complete deep phenotypic and transcriptomic analysis of self-antigen-specific CD4 T cells in human AILD. We analyzed the transcriptomic signature of the CD4 T cell reactivity against three distinct liver-self-antigens and against three common foreign antigens. After a short *in vitro* peptide stimulation, autoreactive CD4 T cells present a common transcriptomic signature

817 although the three self-antigens have no molecular similarity (Sepsecs, CYP2D6 and PDCE2).
818 Interestingly, this transcriptomic signature is distinct from the anti-fungus Th17 (Candida Albicans
819 reactivity) and the anti-viral (influenza H1N1 and Sars-COV2) immune signatures. In our previous
820 publication, we had shown that Sepsecs-specific CD4 T cells, versus the reactive CD4 T cells against the
821 Candida Albicans, have a B-helper / pro-inflammatory immune signature[22]. In this new study, we
822 reinforce the data, and we demonstrate that the immune signature of liver-autoimmunity is clearly
823 distinct from diverse foreign antigen immune responses. The major immune genes characterizing this
824 signature are *TIGIT, CTLA4, NR3C1, TOX, CXCL13, STAT3, PRDM1* and other. This autoreactive signature
825 presents a high similarity with the published signature of the TPH CD4 cell subset described in the
826 tissue of other autoimmune diseases, and also with the phenotype of gluten-specific CD4 T cells in the
827 gut[23,24,29,43]. However, the lack of data available at the single-cell level for other self-antigen-specific
828 CD4 T cells after short peptide stimulation makes it difficult to identify specific genes linked to hepatic
829 autoimmunity in our dataset. Characterizing self-antigen-specific CD4 T cells is not easy, and very few
830 studies have looked at their in-depth immune profiles without an *in vitro* expansion step. For example,
831 Balmas et al have shown that autoreactive CD4 T cells in type 1 diabetes have a pro-inflammatory
832 memory profile characterized by the transcription factor BHLHE40 and the cytokines GM-CSF and TNF-
833 a; this profile diverges from the TPH phenotype[45]. Further work is needed to understand the diversity
834 of autoimmune profiles in different autoimmune disorders. While the TPH signature has been defined
835 by analysis of CD4 T cells in synovial fluids during rheumatoid arthritis (RA), other autoimmune
836 signatures have also been described[23,47]. In RA, multiple sclerosis (MS) and Guillain-Barré syndrome,
837 CD4 T cells with a CTL signature were described[47,49,51]. In MS, CXCR4+ GMCSF+ IL2+ TNF+ CD4 T cells
838 and TFH cells were also associated with disease in the central nervous system[49,52,53].

839 Interestingly, circulating liver-autoreactive CD4 T cells have a profile similar to that of tissue-infiltrating
840 CD4 T cells found in various immune contexts. Expression of PD1, CXCL13, IL21, TIGIT, PRDM1, TOX,
841 CD39, TIM3, CTLA-4, CXCR3, HLA-DR and CXCR6 is commonly shared with the signature of TPH CD4
842 cells in the synovium of RA patients, neoantigen-reactive CD4 T cells in metastatic human cancers,
843 tumor-infiltrating CD4 T cells, liver-infiltrating CD4 T cells in HBV-infected patients and liver-resident
844 CD4 T cells[23,47,54–59]. The main difference is that circulating liver-autoreactive CD4 T cells do not express
845 CD69, which is probably downregulated after tissue egress. Wiggins et al characterized distinct liver-
846 infiltrating CD4 T cells subsets in HLA-disparate liver allografts and they show that CD69 high CD4+ T
847 cells expressing CXCR6 and PD1 are tissue resident cells, which are biased towards interleukin-4 and
848 are not found in the blood[59]. Another CD4 T cells subset expressing an intermediate level of CD69 was
849 described as resident pool also found in the circulation and correlated with liver necroinflammation
850 during chronic hepatitis B infection but not during chronic liver diseases. However, in this study the
851 main criteria to define the retention of CD69 high CD4+ T cells in the liver was based on the expression
852 of CD69, which may decrease outside the tissue in absence of local reactivity. Clonal analysis may be
853 more informative to understand the link between tissue and circulation[36]. In addition, depending on
854 the context of local chronic antigenic reactivity (infection versus chronic inflammation), the immune
855 signature of resident/infiltrating cells may be disrupted, which may explain the differences between
856 different studies and group of patients. For example, during autoimmunity and cancer, tissue-
857 infiltrating CD4 T cells present hallmarks of residency (e.g. CXCR6 and PD1) while their origins are not
858 known with absolute accuracy. We show that liver-autoreactive CD4 T cells present also the hallmarks
859 of residency although they did not express CD69 in the circulation. Thus, the unresolved question is
860 whether local antigen-reactivity depends on local reactivation and clonal expansion of resident cells or
861 on migration of peripheral cells infiltrating the tissue. It is possible that after peripheral activation
862 (following an infection for example), CD4 T cells infiltrate the tissue, where they undergo clonal
863 expansion depending on the antigenic load, and acquire a residency profile[35]. What we can conclude

is that local antigenic reactivity induces a significant modification of CD4 T cells, characterized by the induction of the expression of immune checkpoint molecules and other. These markers found in the peripheral blood may be useful for designing biomarkers related to tissue aggression. Their presence in the blood stream can be explained by the fact that during the active phase of the disease, the high clonal expansion in the liver may favor the recirculation of autoreactive T cells. The high vascularity of the liver and the destruction of the portal structure could explain this leakage into the peripheral bloodstream. This concept is supported by the fact that the frequency of liver-autoreactive CD4 T cells in the blood of patients decreases during the remission phase, which is generally associated with a reduction in intrahepatic lymphocyte activity.

In this study, we were able to identify by flow cytometry an association of markers expressed by circulating liver-autoreactive CD4 T cells, which may be useful for designing relevant biomarkers. We have previously demonstrated that the PD1 and CD38 expression were linked to the AIH activity[22]. Joose et al have demonstrated that TIGIT and CD38 at the surface of circulating CD4 T cells correlated with inflammatory bowel disease activity[60]. Other studies have shown that circulating HLA-DR+ CD38+ CD4 T cells could be useful to quantify T cell activity during immune disorders[61]. PD1, TIGIT, HLA-DR and CD38 are markers expressed by the liver-autoreactive CD4 T cells we have identified in the blood of AILD patients. To go further, we show that the phenotype of these cells is more complex. First the PD1+ TIGIT+ is a heterogeneous subset containing Tregs and cytotoxic T cells, thus Treg exclusion using CD127 and CD25 or FOXP3 expression is important for unbiased analysis. Next, our unsupervised and supervised analyses by using a panel of 22 antibodies were instrumental to establish a complete phenotype of the circulating liver-autoreactive CD4 T cells, as being memory (CD45RA-) CD25- CD127- CXCR5- CCR6- CD57- CD27+ CD49d+ PD1+ TIGIT+ ICOS+ HLA-DR+ CD38+ cells. Intracellular analysis revealed that they are FOXP3- GZMB- and EOMES-. On the basis of these observations and the use of other markers identified after transcriptomic analysis, it will be important to further assess the clinical relevance of possible new biomarkers. For example, direct ex vivo analysis of PD1+ TIGIT+ CXCR5- HLA-DR+ non-Treg CD4 T cells demonstrated that they express high levels of the *CCR2, CCR5, LGALS1, CXCR3* and *CD74* genes compared with other CD4 memory T cell subsets. After TCR stimulation, this subset upregulated CD39, TIM3 and CXCR6 genes relative to other CD4 memory T cell subsets. Taken together, these markers could be useful for delineating liver-derived autoreactive CD4 T cells with high precision.

The major common point between liver-autoreactive CD4 T cells and tissue infiltrating CD4 T cells is the high expression of immune-regulatory molecules (PD-1, TIGIT, CTLA4…), which may be linked to the local chronic antigen reactivity and exhaustion. During cancer, the blockade of PD-1 can restore the activity of tumor-infiltrating CD4 T cells demonstrating their local immune involvement and that immune checkpoint molecules control local reactivity[55,57]. In our study, we demonstrate that immune checkpoint molecules in the liver participate in the local control of antigen-specific T cells. In the absence of immune checkpoint control, CD4 T cell-dependent acute hepatitis is associated with a strong expansion of antigen-specific CD8 T cells. In human, hepatic lesions can be induced by anti-cancer immunotherapy (anti-PD1 and anti-CTLA-4) and are associated with a predominant CD8 T cell infiltrate in the lobular zone, suggesting a reactivation of the local liver-antigen-specific T cell response[62–64]. The major difference with AIH is that during immunotherapy-induced acute hepatitis, no signs of chronicity are reported, and the acute hepatitis is rapidly controlled by immunosuppressive treatments without relapse after treatment withdrawal. During AIH, cytotoxic CD8 T cells are considered the key players in hepatocyte death. CD8 T cells infiltrate the lobular zone where hepatocytes die, and their presence is correlated with disease activity[9,38]. As in immunotherapy-induced acute hepatitis, immunosuppressive therapy abrogates liver degradation and is linked to a drastic reduction in CD8 T cells in the lobular zone. In addition to a CD8 T cell infiltrate in the lobular zone, and in contrast with immunotherapy-induced acute hepatitis, AIH patients' liver biopsies show

911 the complete architecture of a chronic adaptive immune response at diagnosis, which is usually late in
912 the course of the disease. A large number of B cells and of CD4 T cells are observed in the portal
913 zone[63,64]. The detection of tertiary lymphoid structures in the portal zone in our study supports the
914 idea of a prolonged activation period to achieve such immune organization. Moreover, after
915 treatment, it is still possible to detect an infiltrate of CD4 T cells in the portal area[38]. The fact that there
916 are many relapses after discontinuation of treatment suggests the persistence of autoimmune vectors,
917 which could be linked to the chronic immune response of CD4 T cells in the liver. Moreover, we were
918 able to detect persistent self-antigen-specific CD4 T cell clones during three years, suggesting
919 maintenance of clonal expansion rather than renewal following clonal deletion.

920 These differences between acute and chronic hepatitis suggest a possible gradual escape from
921 standard immuno-regulatory processes of the liver-self-antigen-specific T cells during AILD. Studies
922 have shown links between CTLA-4 polymorphisms and susceptibility to AIH and PBC[65–70]. However, the
923 functional biological link with the development of AILD is not known. We can hypothesize that a
924 dysregulation of this pathway participates in the gradual temporal escape of liver-antigen-specific CD4
925 T cell response that mediates the expansion of cytotoxic CD8 T cells. Thus, during chronic autoimmune
926 reactivity, the liver-antigen-specific CD4 T cells may partially escape local control by the immune-
927 checkpoint, which may favor the formation of tertiary lymphoid structure supporting local
928 autoimmunity and damages. Although autoreactive T cells have acquired a signature of exhaustion,
929 which is a hallmark of chronic antigenic reactivity, they are still capable of inducing autoimmune
930 disorders, demonstrating the divergence between the classical exhaustion process and autoreactivity,
931 and suggesting escape mechanisms. In autoimmune rheumatic diseases (SLE and RA), these concepts
932 have been intensively studied, and several genes with risk alleles for rheumatic autoimmunity are
933 linked to T cell activity[71]. Overall, multiple single nucleotide polymorphisms associated with specific T
934 cell regulatory pathways are described in various autoimmune diseases[72]. Therefore, understanding
935 the link between genetic risk and the functional capacity of autoreactive T cells to escape tolerance
936 may open new therapeutic prospects.

937 **References:**

938 1. Webb, G.J., Hirschfield, G.M., Krawitt, E.L., and Gershwin, M.E. (2018). Cellular and Molecular
939 Mechanisms of Autoimmune Hepatitis. Annu. Rev. Pathol. Mech. Dis. *13*, 247–292. 10.1146/annurev-
940 pathol-020117-043534.

941 2. European Association for the Study of the Liver (2015). EASL Clinical Practice Guidelines:
942 Autoimmune hepatitis. J. Hepatol. *63*, 971–1004. 10.1016/j.jhep.2015.06.030.

943 3. Bowlus, C.L., and Gershwin, M.E. (2014). The diagnosis of primary biliary cirrhosis.
944 Autoimmunity Reviews *13*, 441–444. 10.1016/j.autrev.2014.01.041.

945 4. European Association for the Study of the Liver. Electronic address: easloffice@easloffice.eu
946 and European Association for the Study of the Liver (2017). EASL Clinical Practice Guidelines: The
947 diagnosis and management of patients with primary biliary cholangitis. J. Hepatol. *67*, 145–172.
948 10.1016/j.jhep.2017.03.022.

949 5. Poch, T., Krause, J., Casar, C., Liwinski, T., Glau, L., Kaufmann, M., Ahrenstorf, A.E., Hess, L.U.,
950 Ziegler, A.E., Martrus, G., et al. (2021). Single-cell atlas of hepatic T cells reveals expansion of liver-
951 resident naive-like CD4+ T cells in primary sclerosing cholangitis. Journal of Hepatology *75*, 414–423.
952 10.1016/j.jhep.2021.03.016.

953 6. Zimmer, C.L., Von Seth, E., Buggert, M., Strauss, O., Hertwig, L., Nguyen, S., Wong, A.Y.W.,
954 Zotter, C., Berglin, L., Michaëlsson, J., et al. (2021). A biliary immune landscape map of primary
955 sclerosing cholangitis reveals a dominant network of neutrophils and tissue-resident T cells. Sci.
956 Transl. Med. *13*, eabb3107. 10.1126/scitranslmed.abb3107.

957 7. Andrews, T.S., Nakib, D., Perciani, C.T., Ma, X.Z., Liu, L., Winter, E., Camat, D., Chung, S.W.,
958 Lumanto, P., Manuel, J., et al. (2024). Single-cell, single-nucleus, and spatial transcriptomics
959 characterization of the immunological landscape in the healthy and PSC human liver. Journal of
960 Hepatology, S0168827824000035. 10.1016/j.jhep.2023.12.023.

961 8. Sirpal, S., and Chandok, N. (2017). Primary sclerosing cholangitis: diagnostic and management
962 challenges. Clin Exp Gastroenterol *10*, 265–273. 10.2147/CEG.S105872.

963 9. You, Z., Li, Y., Wang, Q., Zhao, Z., Li, Y., Qian, Q., Li, B., Zhang, J., Huang, B., Liang, J., et al.
964 (2021). The Clinical Significance of Hepatic $CD69^+CD103^+CD8^+$ Resident-Memory T Cells in
965 Autoimmune Hepatitis. Hepatology *74*, 847–863. 10.1002/hep.31739.

966 10. Ellinghaus, D. (2022). How genetic risk contributes to autoimmune liver disease. Semin
967 Immunopathol *44*, 397–410. 10.1007/s00281-022-00950-8.

968 11. Chen, H., Han, Z., Fan, Y., Chen, L., Peng, F., Cheng, X., Wang, Y., Su, J., and Li, D. (2023). CD4+
969 T-cell subsets in autoimmune hepatitis: A review. Hepatology Communications *7*.
970 10.1097/HC9.0000000000000269.

971 12. Cardon, A., Conchon, S., and Renand, A. (2021). Mechanisms of autoimmune hepatitis. Curr
972 Opin Gastroenterol *37*, 79–85. 10.1097/MOG.0000000000000704.

973 13. Than, N.N., Hodson, J., Schmidt-Martin, D., Taubert, R., Wawman, R.E., Botter, M., Gautam,
974 N., Bock, K., Jones, R., Appanna, G.D., et al. (2019). Efficacy of rituximab in difficult-to-manage
975 autoimmune hepatitis: Results from the International Autoimmune Hepatitis Group. JHEP Reports *1*,
976 437–445. 10.1016/j.jhepr.2019.10.005.

977 14. Longhi, M.S., Hussain, M.J., Bogdanos, D.P., Quaglia, A., Mieli-Vergani, G., Ma, Y., and
978 Vergani, D. (2007). Cytochrome P450IID6-specific CD8 T cell immune responses mirror disease
979 activity in autoimmune hepatitis type 2. Hepatology *46*, 472–484. 10.1002/hep.21658.

980 15. Löhr, H.F., Schlaak, J.F., Lohse, A.W., Böcher, W.O., Arenz, M., Gerken, G., and Meyer Zum
981 Büschenfelde, K.H. (1996). Autoreactive CD4+ LKM-specific and anticlonotypic T-cell responses in
982 LKM-1 antibody-positive autoimmune hepatitis. Hepatology *24*, 1416–1421.
983 10.1002/hep.510240619.

984 16. Chow, I.-T., James, E.A., Gates, T.J., Tan, V., Moustakas, A.K., Papadopoulos, G.K., and Kwok,
985 W.W. (2013). Differential Binding of Pyruvate Dehydrogenase Complex-E2 Epitopes by DRB1*08:01
986 and DRB1*11:01 Is Predicted by Their Structural Motifs and Correlates with Disease Risk. The Journal
987 of Immunology *190*, 4516–4524. 10.4049/jimmunol.1202445.

988 17. Mix, H., Weiler-Normann, C., Thimme, R., Ahlenstiel, G., Shin, E.-C., Herkel, J., David, C.S.,
989 Lohse, A.W., and Rehermann, B. (2008). Identification of CD4 T-cell epitopes in soluble liver
990 antigen/liver pancreas autoantigen in autoimmune hepatitis. Gastroenterology *135*, 2107–2118.
991 10.1053/j.gastro.2008.07.029.

992 18. Ehser, J., Holdener, M., Christen, S., Bayer, M., Pfeilschifter, J.M., Hintermann, E., Bogdanos,
993 D., and Christen, U. (2013). Molecular mimicry rather than identity breaks T-cell tolerance in the

994 CYP2D6 mouse model for human autoimmune hepatitis. J. Autoimmun. *42*, 39–49.
995 10.1016/j.jaut.2012.11.001.

996 19. Hardtke-Wolenski, M., Fischer, K., Noyan, F., Schlue, J., Falk, C.S., Stahlhut, M., Woller, N.,
997 Kuehnel, F., Taubert, R., Manns, M.P., et al. (2013). Genetic predisposition and environmental danger
998 signals initiate chronic autoimmune hepatitis driven by CD4+ T cells. Hepatology *58*, 718–728.
999 10.1002/hep.26380.

1000 20. Holdener, M., Hintermann, E., Bayer, M., Rhode, A., Rodrigo, E., Hintereder, G., Johnson, E.F.,
1001 Gonzalez, F.J., Pfeilschifter, J., Manns, M.P., et al. (2008). Breaking tolerance to the natural human
1002 liver autoantigen cytochrome P450 2D6 by virus infection. J. Exp. Med. *205*, 1409–1422.
1003 10.1084/jem.20071859.

1004 21. Lapierre, P., Djilali-Saiah, I., Vitozzi, S., and Alvarez, F. (2004). A murine model of type 2
1005 autoimmune hepatitis: Xenoimmunization with human antigens. Hepatology *39*, 1066–1074.
1006 10.1002/hep.20109.

1007 22. Renand, A., Cervera-Marzal, I., Gil, L., Dong, C., Garcia, A., Kervagoret, E., Aublé, H., Habes, S.,
1008 Chevalier, C., Vavasseur, F., et al. (2020). Integrative molecular profiling of autoreactive CD4 T cells in
1009 autoimmune hepatitis. Journal of Hepatology *73*, 1379–1390. 10.1016/j.jhep.2020.05.053.

1010 23. Rao, D.A., Gurish, M.F., Marshall, J.L., Slowikowski, K., Fonseka, C.Y., Liu, Y., Donlin, L.T.,
1011 Henderson, L.A., Wei, K., Mizoguchi, F., et al. (2017). Pathologically expanded peripheral T helper cell
1012 subset drives B cells in rheumatoid arthritis. Nature *542*, 110–114. 10.1038/nature20810.

1013 24. Zhang, F., Wei, K., Slowikowski, K., Fonseka, C.Y., Rao, D.A., Kelly, S., Goodman, S.M.,
1014 Tabechian, D., Hughes, L.B., Salomon-Escoto, K., et al. (2019). Defining inflammatory cell states in
1015 rheumatoid arthritis joint synovial tissues by integrating single-cell transcriptomics and mass
1016 cytometry. Nat. Immunol. *20*, 928–942. 10.1038/s41590-019-0378-1.

1017 25. Marks, K.E., and Rao, D.A. (2022). T peripheral helper cells in autoimmune diseases*.
1018 Immunological Reviews *307*, 191–202. 10.1111/imr.13069.

1019 26. Arazi, A., Rao, D.A., Berthier, C.C., Davidson, A., Liu, Y., Hoover, P.J., Chicoine, A., Eisenhaure,
1020 T.M., Jonsson, A.H., Li, S., et al. (2019). The immune cell landscape in kidneys of patients with lupus
1021 nephritis. Nat. Immunol. *20*, 902–914. 10.1038/s41590-019-0398-x.

1022 27. Han, D., Lee, A.Y., Kim, T., Choi, J.Y., Cho, M.Y., Song, A., Kim, C., Shim, J.H., Kim, H.J., Kim, H.,
1023 et al. (2023). Microenvironmental network of clonal CXCL13+CD4+ T cells and Tregs in pemphigus
1024 chronic blisters. Journal of Clinical Investigation *133*, e166357. 10.1172/JCI166357.

1025 28. Harada, T., Kikushige, Y., Miyamoto, T., Uno, K., Niiro, H., Kawakami, A., Koga, T., Akashi, K.,
1026 and Yoshizaki, K. (2023). Peripheral helper-T-cell-derived CXCL13 is a crucial pathogenic factor in
1027 idiopathic multicentric Castleman disease. Nat Commun *14*, 6959. 10.1038/s41467-023-42718-0.

1028 29. Christophersen, A., Lund, E.G., Snir, O., Solà, E., Kanduri, C., Dahal-Koirala, S., Zühlke, S.,
1029 Molberg, Ø., Utz, P.J., Rohani-Pichavant, M., et al. (2019). Distinct phenotype of CD4+ T cells driving
1030 celiac disease identified in multiple autoimmune conditions. Nat. Med. *25*, 734–737.
1031 10.1038/s41591-019-0403-9.

1032 30. Yong, L., Chunyan, W., Yan, Y., Wanyu, L., Huifan, J., Pingwei, Z., and Yanfang, J. (2021).
1033 Expanded circulating peripheral helper T cells in primary biliary cholangitis. Molecular Immunology
1034 *131*, 44–50. 10.1016/j.molimm.2020.09.007.

1035 31. Kita, H., Matsumura, S., He, X.-S., Ansari, A.A., Lian, Z.-X., Van de Water, J., Coppel, R.L.,
1036 Kaplan, M.M., and Gershwin, M.E. (2002). Quantitative and functional analysis of PDC-E2–specific
1037 autoreactive cytotoxic T lymphocytes in primary biliary cirrhosis. J. Clin. Invest. *109*, 1231–1240.
1038 10.1172/JCI0214698.

1039 32. Van de Water, J., Ansari, A., Prindiville, T., Coppel, R.L., Ricalton, N., Kotzin, B.L., Liu, S.,
1040 Roche, T.E., Krams, S.M., Munoz, S., et al. (1995). Heterogeneity of autoreactive T cell clones specific
1041 for the E2 component of the pyruvate dehydrogenase complex in primary biliary cirrhosis. J Exp Med
1042 *181*, 723–733. 10.1084/jem.181.2.723.

1043 33. Shimoda, S., Ishikawa, F., Kamihira, T., Komori, A., Niiro, H., Baba, E., Harada, K., Isse, K.,
1044 Nakanuma, Y., Ishibashi, H., et al. (2006). Autoreactive T-Cell Responses in Primary Biliary Cirrhosis
1045 Are Proinflammatory Whereas Those of Controls Are Regulatory. Gastroenterology *131*, 606–618.
1046 10.1053/j.gastro.2006.05.056.

1047 34. Bovensiepen, C.S., Schakat, M., Sebode, M., Zenouzi, R., Hartl, J., Peiseler, M., Li, J., Henze, L.,
1048 Woestemeier, A., Schramm, C., et al. (2019). TNF-Producing Th1 Cells Are Selectively Expanded in
1049 Liver Infiltrates of Patients with Autoimmune Hepatitis. J. Immunol. *203*, 3148–3156.
1050 10.4049/jimmunol.1900124.

1051 35. Nguyen, Q.P., Takehara, K.K., Deng, T.Z., O'Shea, S., Heeg, M., Omilusik, K.D., Milner, J.J.,
1052 Quon, S., Pipkin, M.E., Choi, J., et al. (2023). Transcriptional programming of $CD4^+ T_{RM}$ differentiation
1053 in viral infection balances effector- and memory-associated gene expression. Sci. Immunol. *8*,
1054 eabq7486. 10.1126/sciimmunol.abq7486.

1055 36. Poon, M.M.L., Caron, D.P., Wang, Z., Wells, S.B., Chen, D., Meng, W., Szabo, P.A., Lam, N.,
1056 Kubota, M., Matsumoto, R., et al. (2023). Tissue adaptation and clonal segregation of human memory
1057 T cells in barrier sites. Nat Immunol *24*, 309–319. 10.1038/s41590-022-01395-9.

1058 37. Hennes, E.M., Zeniya, M., Czaja, A.J., Parés, A., Dalekos, G.N., Krawitt, E.L., Bittencourt, P.L.,
1059 Porta, G., Boberg, K.M., Hofer, H., et al. (2008). Simplified criteria for the diagnosis of autoimmune
1060 hepatitis. Hepatology *48*, 169–176. 10.1002/hep.22322.

1061 38. Renand, A., Habes, S., Mosnier, J.-F., Aublé, H., Judor, J.-P., Vince, N., Hulin, P., Nedellec, S.,
1062 Métairie, S., Archambeaud, I., et al. (2018). Immune Alterations in Patients With Type 1 Autoimmune
1063 Hepatitis Persist Upon Standard Immunosuppressive Treatment. Hepatol Commun *2*, 968–981.
1064 10.1002/hep4.1202.

1065 39. Attaf, N., Cervera-Marzal, I., Dong, C., Gil, L., Renand, A., Spinelli, L., and Milpied, P. (2020).
1066 FB5P-seq: FACS-Based 5-Prime End Single-Cell RNA-seq for Integrative Analysis of Transcriptome and
1067 Antigen Receptor Repertoire in B and T Cells. Front. Immunol. *11*, 216. 10.3389/fimmu.2020.00216.

1068 40. Hahaut, V., Pavlinic, D., Carbone, W., Schuierer, S., Balmer, P., Quinodoz, M., Renner, M.,
1069 Roma, G., Cowan, C.S., and Picelli, S. (2022). Fast and highly sensitive full-length single-cell RNA
1070 sequencing using FLASH-seq. Nat Biotechnol *40*, 1447–1451. 10.1038/s41587-022-01312-3.

1071 41. Yossef, R., Krishna, S., Sindiri, S., Lowery, F.J., Copeland, A.R., Gartner, J.J., Parkhurst, M.R.,
1072 Parikh, N.B., Hitscherich, K.J., Levi, S.T., et al. (2023). Phenotypic signatures of circulating neoantigen-
1073 reactive CD8+ T cells in patients with metastatic cancers. Cancer Cell *41*, 2154-2165.e5.
1074 10.1016/j.ccell.2023.11.005.

1075 42. Parekh, S., Ziegenhain, C., Vieth, B., Enard, W., and Hellmann, I. (2018). zUMIs - A fast and
1076 flexible pipeline to process RNA sequencing data with UMIs. GigaScience *7*.
1077 10.1093/gigascience/giy059.

1078 43. Bocharnikov, A.V., Keegan, J., Wacleche, V.S., Cao, Y., Fonseka, C.Y., Wang, G., Muise, E.S.,
1079 Zhang, K.X., Arazi, A., Keras, G., et al. (2019). PD-1hiCXCR5- T peripheral helper cells promote B cell
1080 responses in lupus via MAF and IL-21. JCI Insight *4*. 10.1172/jci.insight.130062.

1081 44. Song, L., Cohen, D., Ouyang, Z., Cao, Y., Hu, X., and Liu, X.S. (2021). TRUST4: immune
1082 repertoire reconstruction from bulk and single-cell RNA-seq data. Nat Methods *18*, 627–630.
1083 10.1038/s41592-021-01142-2.

1084 45. Balmas, E., Chen, J., Hu, A.K., DeBerg, H.A., Rosasco, M.G., Gersuk, V.H., Serti, E., Speake, C.,
1085 Greenbaum, C.J., Nepom, G.T., et al. (2023). Islet-autoreactive CD4+ T cells are linked with response
1086 to alefacept in type 1 diabetes. JCI Insight *8*, e167881. 10.1172/jci.insight.167881.

1087 46. Hao, Y., Hao, S., Andersen-Nissen, E., Mauck, W.M., Zheng, S., Butler, A., Lee, M.J., Wilk, A.J.,
1088 Darby, C., Zager, M., et al. (2021). Integrated analysis of multimodal single-cell data. Cell *184*, 3573-
1089 3587.e29. 10.1016/j.cell.2021.04.048.

1090 47. Argyriou, A., Wadsworth, M.H., Lendvai, A., Christensen, S.M., Hensvold, A.H., Gerstner, C.,
1091 Van Vollenhoven, A., Kravarik, K., Winkler, A., Malmström, V., et al. (2022). Single cell sequencing
1092 identifies clonally expanded synovial CD4+ TPH cells expressing GPR56 in rheumatoid arthritis. Nat
1093 Commun *13*, 4046. 10.1038/s41467-022-31519-6.

1094 48. Korsunsky, I., Millard, N., Fan, J., Slowikowski, K., Zhang, F., Wei, K., Baglaenko, Y., Brenner,
1095 M., Loh, P., and Raychaudhuri, S. (2019). Fast, sensitive and accurate integration of single-cell data
1096 with Harmony. Nat Methods *16*, 1289–1296. 10.1038/s41592-019-0619-0.

1097 49. Schafflick, D., Xu, C.A., Hartlehnert, M., Cole, M., Schulte-Mecklenbeck, A., Lautwein, T.,
1098 Wolbert, J., Heming, M., Meuth, S.G., Kuhlmann, T., et al. (2020). Integrated single cell analysis of
1099 blood and cerebrospinal fluid leukocytes in multiple sclerosis. Nat Commun *11*, 247. 10.1038/s41467-
1100 019-14118-w.

1101 50. Ishak, K., Baptista, A., Bianchi, L., Callea, F., De Groote, J., Gudat, F., Denk, H., Desmet, V.,
1102 Korb, G., and MacSween, R.N. (1995). Histological grading and staging of chronic hepatitis. J. Hepatol.
1103 *22*, 696–699.

1104 51. Súkeníková, L., Mallone, A., Schreiner, B., Ripellino, P., Nilsson, J., Stoffel, M., Ulbrich, S.E.,
1105 Sallusto, F., and Latorre, D. (2024). Autoreactive T cells target peripheral nerves in Guillain–Barré
1106 syndrome. Nature *626*, 160–168. 10.1038/s41586-023-06916-6.

1107 52. Galli, E., Hartmann, F.J., Schreiner, B., Ingelfinger, F., Arvaniti, E., Diebold, M., Mrdjen, D., Van
1108 Der Meer, F., Krieg, C., Nimer, F.A., et al. (2019). GM-CSF and CXCR4 define a T helper cell signature
1109 in multiple sclerosis. Nat Med *25*, 1290–1300. 10.1038/s41591-019-0521-4.

1110 53. Ostkamp, P., Deffner, M., Schulte-Mecklenbeck, A., Wünsch, C., Lu, I.-N., Wu, G.F., Goelz, S.,
1111 De Jager, P.L., Kuhlmann, T., Gross, C.C., et al. (2022). A single-cell analysis framework allows for
1112 characterization of CSF leukocytes and their tissue of origin in multiple sclerosis. Sci. Transl. Med. *14*,
1113 eadc9778. 10.1126/scitranslmed.adc9778.

1114 54. Lowery, F.J., Krishna, S., Yossef, R., Parikh, N.B., Chatani, P.D., Zacharakis, N., Parkhurst, M.R.,
1115 Levin, N., Sindiri, S., Sachs, A., et al. (2022). Molecular signatures of antitumor neoantigen-reactive T
1116 cells from metastatic human cancers. Science *375*, 877–884. 10.1126/science.abl5447.

1117 55. Balança, C.-C., Salvioni, A., Scarlata, C.-M., Michelas, M., Martinez-Gomez, C., Gomez-Roca,
1118 C., Sarradin, V., Tosolini, M., Valle, C., Pont, F., et al. (2021). PD-1 blockade restores helper activity of
1119 tumor-infiltrating, exhausted PD-1hiCD39+ CD4 T cells. JCI Insight *6*, e142513.
1120 10.1172/jci.insight.142513.

1121 56. Duhen, R., Fesneau, O., Samson, K.A., Frye, A.K., Beymer, M., Rajamanickam, V., Ross, D.,
1122 Tran, E., Bernard, B., Weinberg, A.D., et al. (2022). PD-1 and ICOS coexpression identifies tumor-
1123 reactive CD4+ T cells in human solid tumors. Journal of Clinical Investigation *132*, e156821.
1124 10.1172/JCI156821.

1125 57. Magen, A., Hamon, P., Fiaschi, N., Soong, B.Y., Park, M.D., Mattiuz, R., Humblin, E., Troncoso,
1126 L., D'souza, D., Dawson, T., et al. (2023). Intratumoral dendritic cell–CD4+ T helper cell niches enable
1127 CD8+ T cell differentiation following PD-1 blockade in hepatocellular carcinoma. Nat Med *29*, 1389–
1128 1399. 10.1038/s41591-023-02345-0.

1129 58. Zhang, C., Li, J., Cheng, Y., Meng, F., Song, J.-W., Fan, X., Fan, H., Li, J., Fu, Y.-L., Zhou, M.-J., et
1130 al. (2023). Single-cell RNA sequencing reveals intrahepatic and peripheral immune characteristics
1131 related to disease phases in HBV-infected patients. Gut *72*, 153–167. 10.1136/gutjnl-2021-325915.

1132 59. Wiggins, B.G., Pallett, L.J., Li, X., Davies, S.P., Amin, O.E., Gill, U.S., Kucykowicz, S., Patel, A.M.,
1133 Aliazis, K., Liu, Y.S., et al. (2022). The human liver microenvironment shapes the homing and function
1134 of $CD4^+$ T-cell populations. Gut *71*, 1399–1411. 10.1136/gutjnl-2020-323771.

1135 60. Joosse, M.E., Menckeberg, C.L., De Ruiter, L.F., Raatgeep, H. (Rolien) C., Van Berkel, L.A.,
1136 Simons-Oosterhuis, Y., Tindemans, I., Muskens, A. (Femke) M., Hendriks, R.W., Hoogenboezem, R.M.,
1137 et al. (2019). Frequencies of circulating regulatory TIGIT+CD38+ effector T cells correlate with the
1138 course of inflammatory bowel disease. Mucosal Immunology *12*, 154–163. 10.1038/s41385-018-
1139 0078-4.

1140 61. Nguyen, T.H., Kumar, D., Prince, C., Martini, D., Grunwell, J.R., Lawrence, T., Whitely, T.,
1141 Chappelle, K., Chonat, S., Prahalad, S., et al. (2024). Frequency of HLA-DR+CD38hi T cells identifies
1142 and quantifies T-cell activation in hemophagocytic lymphohistiocytosis, hyperinflammation, and
1143 immune regulatory disorders. Journal of Allergy and Clinical Immunology *153*, 309–319.
1144 10.1016/j.jaci.2023.07.008.

1145 62. De Martin, E., Michot, J.-M., Papouin, B., Champiat, S., Mateus, C., Lambotte, O., Roche, B.,
1146 Antonini, T.M., Coilly, A., Laghouati, S., et al. (2018). Characterization of liver injury induced by cancer
1147 immunotherapy using immune checkpoint inhibitors. J. Hepatol. *68*, 1181–1190.
1148 10.1016/j.jhep.2018.01.033.

1149 63. Zen, Y., and Yeh, M.M. (2018). Hepatotoxicity of immune checkpoint inhibitors: a histology
1150 study of seven cases in comparison with autoimmune hepatitis and idiosyncratic drug-induced liver
1151 injury. Modern Pathology *31*, 965–973. 10.1038/s41379-018-0013-y.

1152 64. Hagiwara, S., Watanabe, T., Kudo, M., Minaga, K., Komeda, Y., Kamata, K., Kimura, M.,
1153 Hayashi, H., Nakagawa, K., Ueshima, K., et al. (2021). Clinicopathological analysis of hepatic immune-
1154 related adverse events in comparison with autoimmune hepatitis and graft-versus host disease. Sci
1155 Rep *11*, 9242. 10.1038/s41598-021-88824-1.

1156 65. Li, Y., Sun, Y., Liu, Y., Wang, B., Li, J., Wang, H., Zhang, H., Wang, X., Han, X., Lin, Q., et al.
1157 (2022). Genome-wide meta-analysis identifies susceptibility loci for autoimmune hepatitis type 1.
1158 Hepatology *76*, 564–575. 10.1002/hep.32417.

1159 66. Agarwal, K., Czaja, A.J., Jones, D.E., and Donaldson, P.T. (2000). Cytotoxic T lymphocyte
1160 antigen-4 (CTLA-4) gene polymorphisms and susceptibility to type 1 autoimmune hepatitis.
1161 Hepatology *31*, 49–53. 10.1002/hep.510310110.

1162 67. Agarwal, K., Jones, D.E., Daly, A.K., James, O.F., Vaidya, B., Pearce, S., and Bassendine, M.F.
1163 (2000). CTLA-4 gene polymorphism confers susceptibility to primary biliary cirrhosis. J Hepatol *32*,
1164 538–541. 10.1016/s0168-8278(00)80213-5.

1165 68. Juran, B.D., Atkinson, E.J., Schlicht, E.M., Fridley, B.L., Petersen, G.M., and Lazaridis, K.N.
1166 (2007). Interacting alleles of the coinhibitory immunoreceptor genes cytotoxic T-lymphocyte antigen
1167 4 and programmed cell-death 1 influence risk and features of primary biliary cirrhosis. Hepatology
1168 *47*, 563–570. 10.1002/hep.22048.

1169 69. Joshita, S., Umemura, T., Yoshizawa, K., Katsuyama, Y., Tanaka, E., Nakamura, M., Ishibashi,
1170 H., Ota, M., and Shinshu PBC Study Group (2010). Association analysis of cytotoxic T-lymphocyte
1171 antigen 4 gene polymorphisms with primary biliary cirrhosis in Japanese patients. J Hepatol *53*, 537–
1172 541. 10.1016/j.jhep.2010.03.017.

1173 70. Qin, B., Li, J., Liang, Y., Yang, Z., and Zhong, R. (2014). The association between Cytotoxic T
1174 Lymphocyte Associated Antigen-4, Fas, Tumour Necrosis Factor-α gene polymorphisms and
1175 autoimmune hepatitis: A meta-analysis. Digestive and Liver Disease *46*, 541–548.
1176 10.1016/j.dld.2014.02.003.

1177 71. Rosetti, F., Madera-Salcedo, I.K., Rodríguez-Rodríguez, N., and Crispín, J.C. (2022). Regulation
1178 of activated T cell survival in rheumatic autoimmune diseases. Nat Rev Rheumatol *18*, 232–244.
1179 10.1038/s41584-021-00741-9.

1180 72. Lagattuta, K.A., Park, H.L., Rumker, L., Ishigaki, K., Nathan, A., and Raychaudhuri, S. (2024).
1181 The genetic basis of autoimmunity seen through the lens of T cell functional traits. Nat Commun *15*,
1182 1204. 10.1038/s41467-024-45170-w.

1183